This is to certify that the

thesis entitled

THE MICHIGAMME INTRUSION, A CASE STUDY OF THE IMPORTANCE OF REMANENT MAGNETIZATION IN MAGNETIC INTERPRETATIONS, MARQUETTE COUNTY, MICHIGAN.

presented by

Wesley M. Phillips

has been accepted towards fulfillment of the requirements for

M.S. degree in GEOLOGY

Thomas A. Vogel
Major professor

Date 8/2/79

THE MICHIGAMME INTRUSION, A CASE STUDY OF THE IMPORTANCE OF REMANENT MAGNETIZATION IN MAGNETIC INTERPRETATIONS, MARQUETTE COUNTY, MICHIGAN

By

Wesley M. Phillips

A THESIS

Submitted to
Michigan State University
in partial fulfillment of the requirements
for the degree of

MASTER OF SCIENCE

Department of Geology

1979

ABSTRACT

THE MICHIGAMME INTRUSION, A CASE STUDY OF THE IMPORTANCE OF REMANENT MAGNETIZATION IN MAGNETIC INTERPRETATIONS, MARQUETTE COUNTY, MICHIGAN

By

Wesley M. Phillips

A computerized magnetic modeling study of the Michigamme Intrusion is performed to demonstrate the importance of natural remanent magnetization (NRM) in magnetic interpretations, and to exhibit the ease with which NRM can be considered with the aid of a computer program. The structure of the intrusion is magnetically modeled by comparing the observed vertical magnetic anomaly of the intrusion to vertical magnetic anomalies generated by computer models of the intrusion. Analysis of the magnetic properties of the body show the intrusion to possess a predominately large reverse-remanent magnetization component. Computer models show that the observed magnetic anomaly of the intrusion is easily modeled, given the geophysical and geologic parameters determined in the study, as a stock steeply dipping to the north. It is also shown that approximate models considering NRM can be made without a detailed field analysis of the body by using paleopole orientations as an approximation of the NRM orientation.

ACKNOWLEDGMENTS

My sincere thanks go:

to Tom Vogel without whom this study would never have been completed. Thank you for your patience and understanding.

to my committee, Dr. H. Bennett, Dr. F. W. Cambray, Dr. J. Wilband for their assistance. Special thanks to John for his help with the computer.

to Dr. R. Vandervoo of the University of Michigan for the use of his paleomagnetic laboratory and equipment. Special thanks to Doyle Watts for his assistance with the equipment.

to Paul Tipler and Bob Williamson of Oakland University for their cherished friendship and stimulation in the sciences.

to Mark Schoomaker and Tim Stanton for their help with the field work. Also special thanks to Mark for his invaluable assistance with the computer programming.

to the Chateau for providing a home from which things such as this can be done without one going off the deep end; and to my friends, one and all.

to my family for their love and understanding.

TABLE OF CONTENTS

LIST OF TABLES

LIST OF FIGURES

Figure | Page

INTRODUCTION

The purpose of this study is to present a magnetic modeling study of the Michigamme Intrusion to show the importance of natural remanent magnetization (NRM) in magnetic interpretations; and to exhibit the ease with which NRM can be considered with the aid of a computer program. The structure of the Michigamme Intrusion will be magnetically modeled by comparing the observed vertical magnetic anomaly of the intrusion to vertical magnetic anomalies generated by computer models of the intrusion. The Michigamme Intrusion was selected for this study because of its structure (Stock) and its observable reverse-remanent magnetization component.

In the interpretation of magnetic anomalies the importance of NRM is gradually being accepted. Early theoretical investigators (Zietz and Brooks, 1951; Sutton and Mumme, 1957; Hood, 1963; Zietz and Andreasen, 1967) indicated that NRM is a significant factor that should be considered in aeromagnetic interpretations. Girdler and Peter (1960) and Torres (1976) showed that some magnetic anomalies cannot be explained by induced magnetization alone and that a large reverse remanent magnetization must be assumed to explain the anomaly under investigation. Other studies have confirmed the importance of NRM in magnetic modeling through interpretation techniques which included direct measurements of the intensity and orientation of the NRM component in the body being studied (Green, 1960; Watkins, 1961; Book, 1962; Hayes and Scharon, 1963; Dubois and Carey, 1964, Strangeway, 1965; Park, 1968).

Most magnetic interpretations do not consider NRM, even though the influence of NRM on magnetic anomalies has been shown. It is the contention of the author that NRM is neglected in magnetic modeling for two simple, but presently unfounded, reasons:

1) The intensity and orientation of the NRM component are not easily available (Green, 1960; Watkins, 1961; Book, 1962; Hayes and Scharon, 1963; Dubois and Carey, 1964; Strangeway, 1965; Park, 1968) or as in some cases not physically obtainable (Girdler, 1960; Torres, 1976).
2) Until recently, computer automated interpretation techniques using induced magnetization (Henderson, 1960; Whitehill, 1973) have not been revised to consider NRM (Shanabrook, 1978).

Location and Topography

The study area is located (Figure 1) in the Upper Peninsula of Michigan approximately one mile west of Champion just off of highway 41. The survey area is contained within sections 25, 26, 35, and 36 of T48N, R30W of the Michigamme and Champion quadrangles, Marquette County.

The intrusion lies on the east shore of Lake Michigamme within sections 35 and 36. The exposure is approximately 1000 feet in diameter and is outlined by a gently sloping, 100 feet topographic high. Outcrop exposures are distributed randomly across the topographic high, but are mostly found intact along the slopes.

Figure 1. Location and Topographic Map.

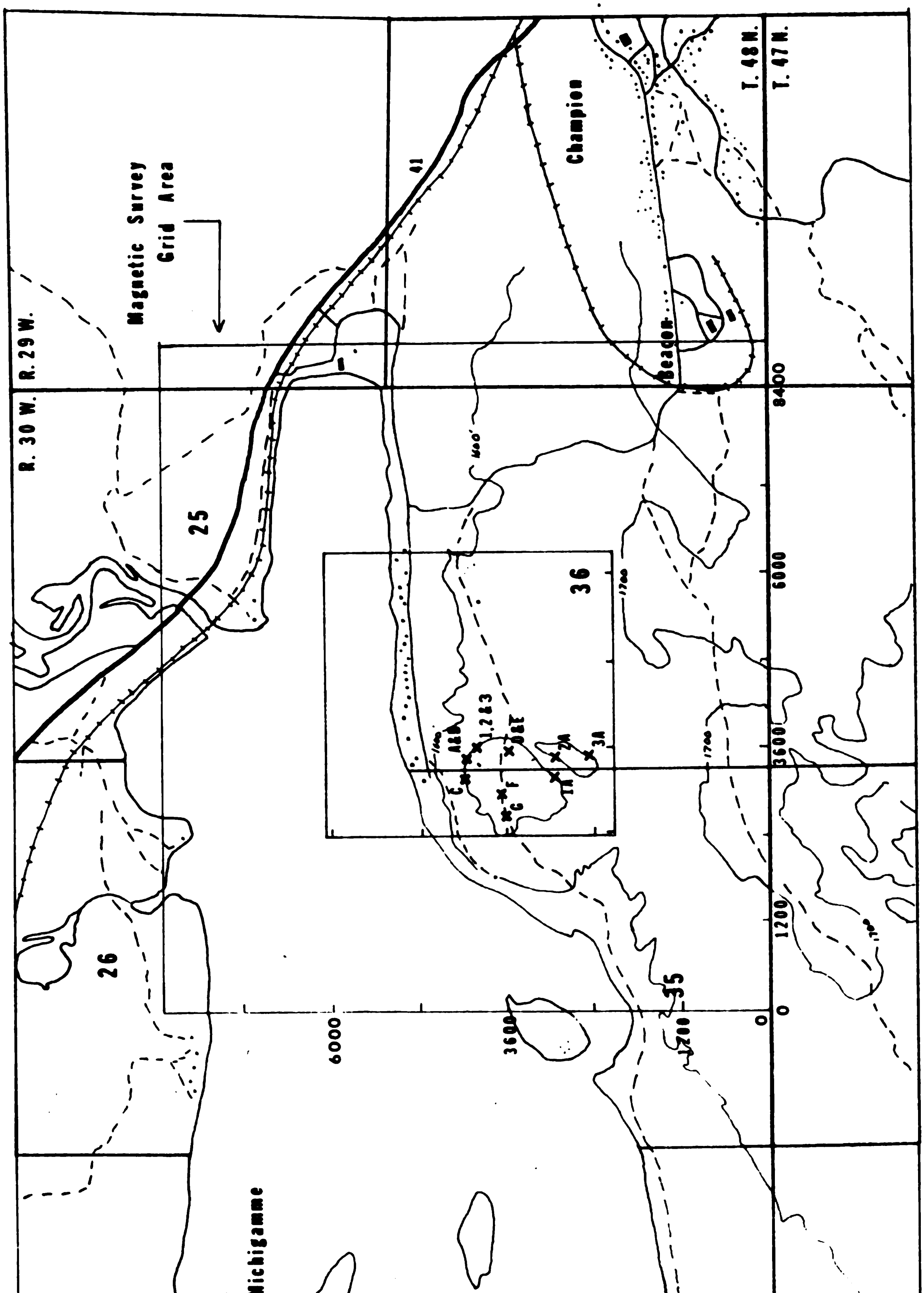
Magnetic Survey Grid Area
R. 30 W.
R. 29 W.
T. 48 N.
T. 47 N.
Champion
Beacon
Lake Michigamme
25
26
35
36
41
0
1200
3600
6000
8400
1700

General Geology and Geophysics

The Michigamme Intrusion is magnetically associated with a swarm of East- West trending dikes. Because the dikes cut structural features of Middle and Lower Precambrian age and are fresh in character, they are considered to be Keweenawan in age (Bodwell, 1972; Wood, 1972). They are classified lower Keweenawan because they are reversely polarized. It is proposed that they were emplaced 1.1 b.y. ago during a period of continental rifting (Chase and Gilmer, 1973).

As shown in Figure 2, the Michigamme intrusion is circular and is located at the Western end of the Marquette Synclinorium where the tightly folded trough begins to open into a broad basin. It transects a series of deformed Middle Precambrian metasediments which belong to the Menominee and Baraga Groups of the Marquette Range Supergroup, (See Cannon and Gairs (1970) revised stratigraphic nomenclature). Gravity profiles indicate depths to basement ranging from a maximum of 2,438 m in the East trough near Humbolt to a maximum of 1,097 m West of Lake Michigamme in the West trough, with the depths becoming shallower toward each end of the trough (Klasner and Cannon, 1974). Deformation in the trough is attributed to the Penokean Orogony (Cannon, 1973), which ocurred 1.85 - 1.95 b.y. ago (VanSchmus, 1970).

Klasner (1972) describes the body as petrographically fresh and zoned containing a mafic pyroxene-rich interior and a plagioclase-rich border phase. Petrographic and chemical analysis of three samples from seperate sites within the interior of the body by Morris (1978), show the intrusion to be a diabase (See Appendix A).

The Total Field, Aeromagnetic map of the general study area reveals a system of intense irregular shaped positive magnetic anomalies and a series of moderate East-West trending positive and negative magnetic

Figure 2. Structural Geologic map of the Lake Michigamme Area (Klasner, 1978).

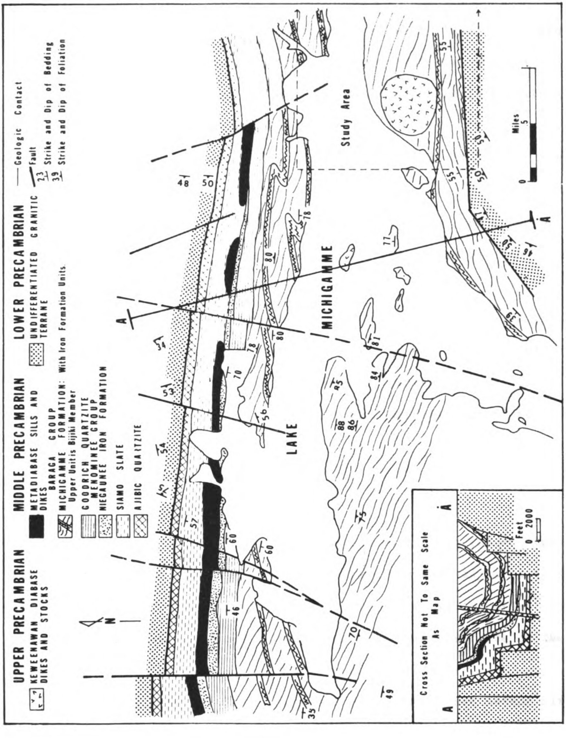
UPPER PRECAMBRIAN
KEWEENAWAN DIABASE DIKES AND STOCKS
MIDDLE PRECAMBRIAN
METADIABASE SILLS AND DIKES
BARAGA GROUP
MICHIGAMME FORMATION: With Iron Formation Units. Upper Unit is Bijiki Member
GOODRICH QUARTZITE
MENOMINEE GROUP
NEGAUNEE IRON FORMATION
SIAMO SLATE
AJIBIC QUARTZITE
LOWER PRECAMBRIAN
UNDIFFERENTIATED GRANITIC TERRANE
Geologic Contact
Fault
Strike and Dip of Bedding
Strike and Dip of Foliation
N
LAKE
MICHIGAMME
Study Area
Miles
0 5
A
A'
Cross Section Not To Same Scale As Map
Feet
0 2000

anomalies (Case and Gair, 1965). The intense positive magnetic anomalies outline the pattern described by the synclinorium and are due to the Negaunee Iron Formation and are also due to the iron-formations contained in the Michigamme Formation. The moderate East-West trending positive magnetic anomalies are due to the metadiabases, while the negative East-West trending magnetic anomalies are associated with reversely polarized Keweenawan Diabases.

The Keweenawan Diabase Stock under investigation is located between East-West striking iron-formations which dip toward the stock (Figure 2). The negative magnetic anomaly associated with the stock may be partially masked by the intense positive magnetic anomalies due to the surrounding iron-formations (Figure 3).

To study the magnetic anomaly of the stock more closely, a ground magnetic survey was conducted. Figure 4 is a general magnetic map of the area which includes part of the anomalies produced by the nearby iron-formations. Figure 5 is a more detailed magnetic map of the anomaly produced by the stock.

Field and Laboratory Methods

The ground magnetic survey was conducted using a Scintrex Flux-Gate Magnetometer (Model MF-2-100). Magnetic readings were adjusted to base stations which were reread approximately every 2 hours to correct for diurnal variations, instrument drift, and temperature effects on the instrument. The adjusted data is listed in Appendix B.

The survey grid was laid out by the pace and compass method with north- south, east-west trending traverses set 600 feet apart (Figure 6). Depending on the amount of detail desired, station spacing within the traverses were varied from 50 feet to 400 feet.

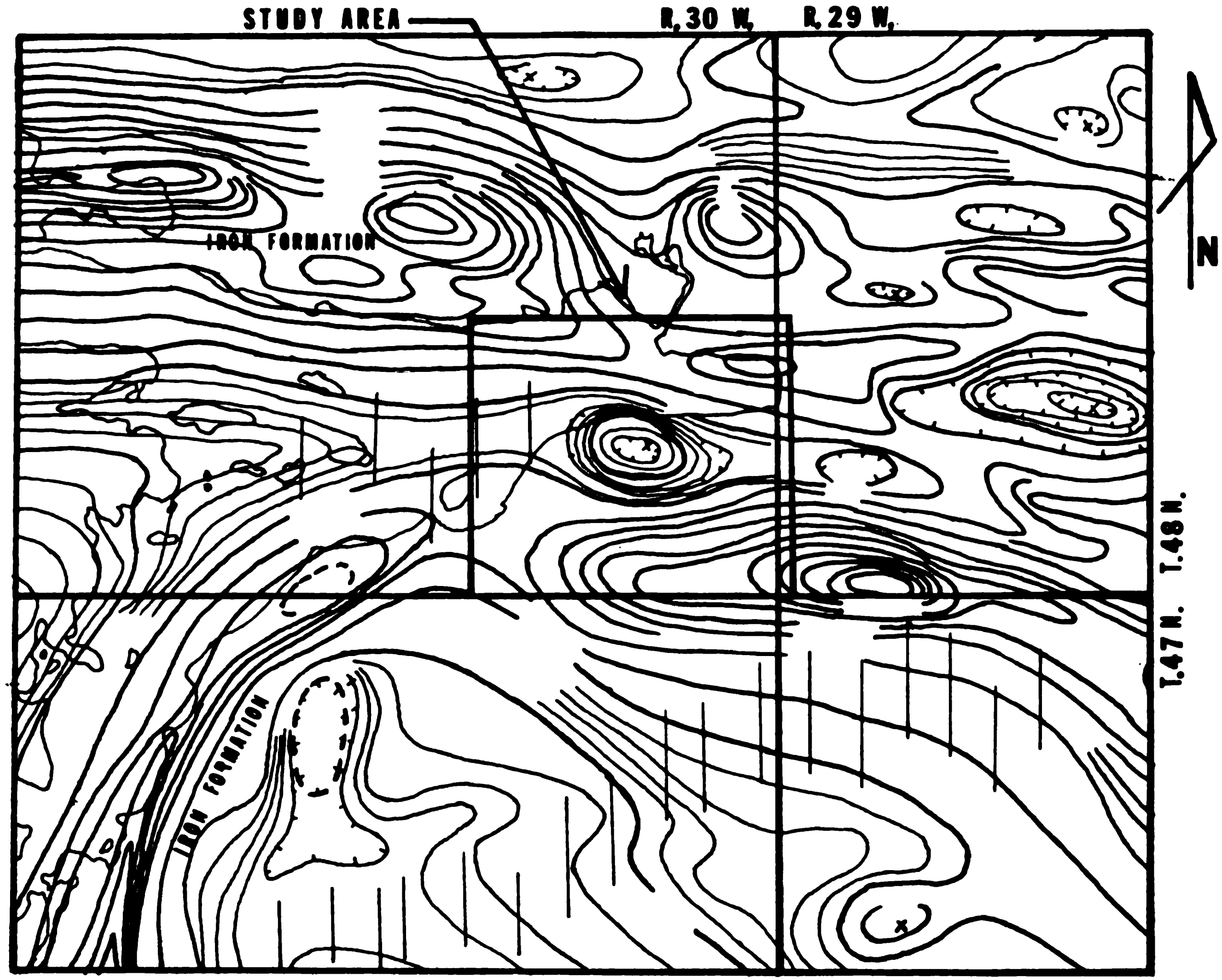

Figure 3. Total intensity, Aeromagnetic map of the study area (Case and Gair, 1965).

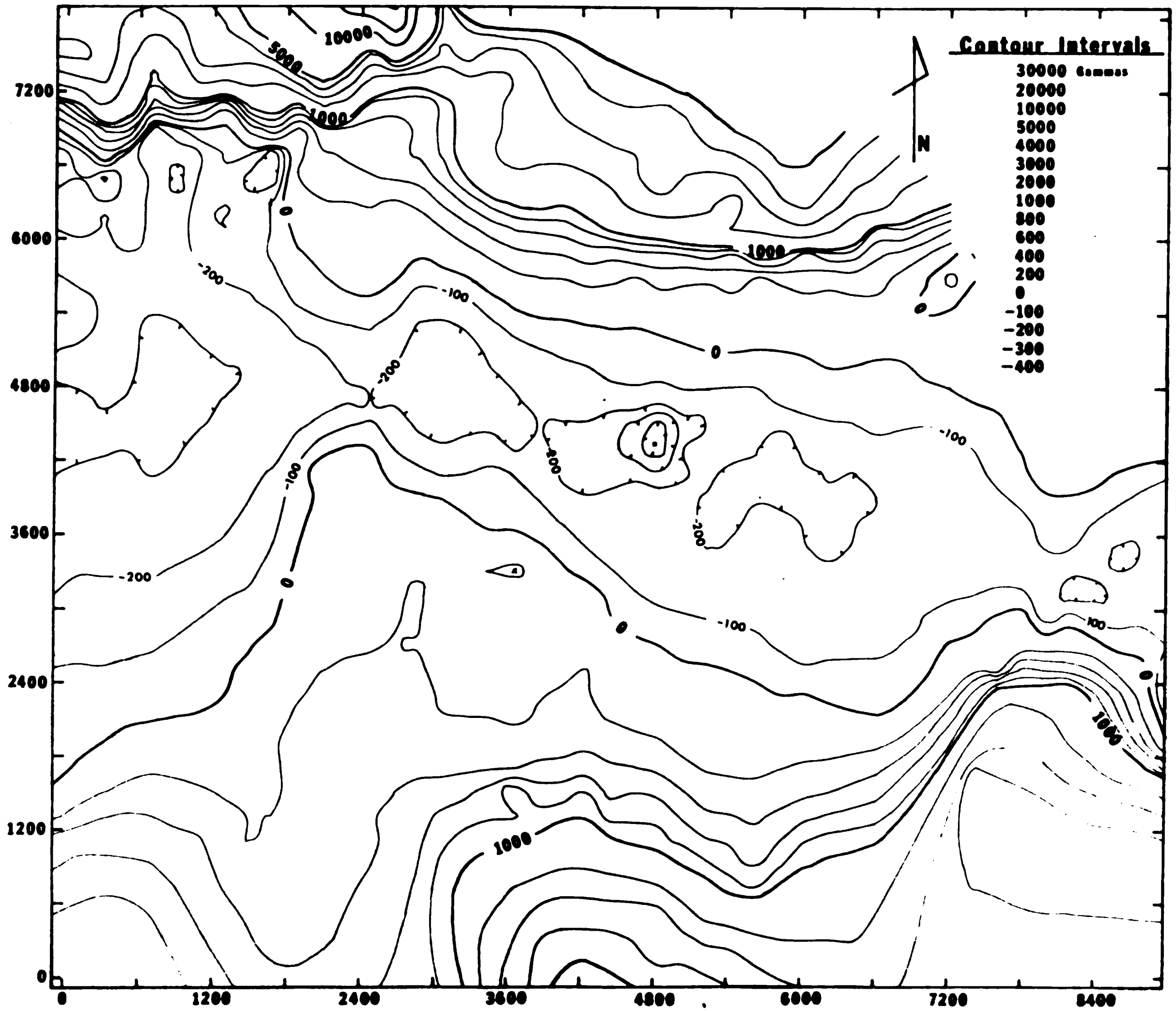

Figure 4. Vertical magnetic intensity contour map (General study area).

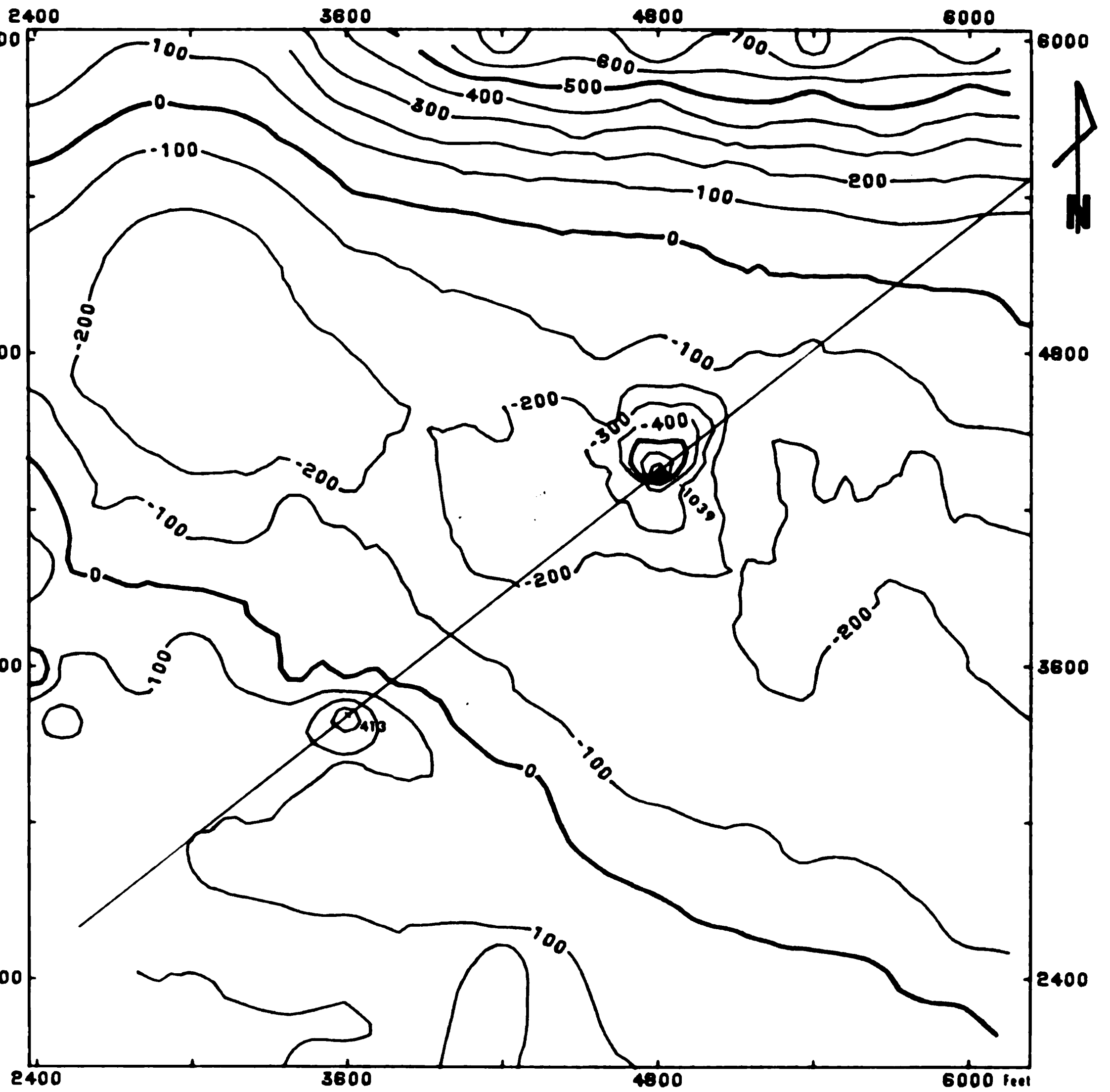

Figure 5. Vertical magnetic intensity contour map (Detailed map).

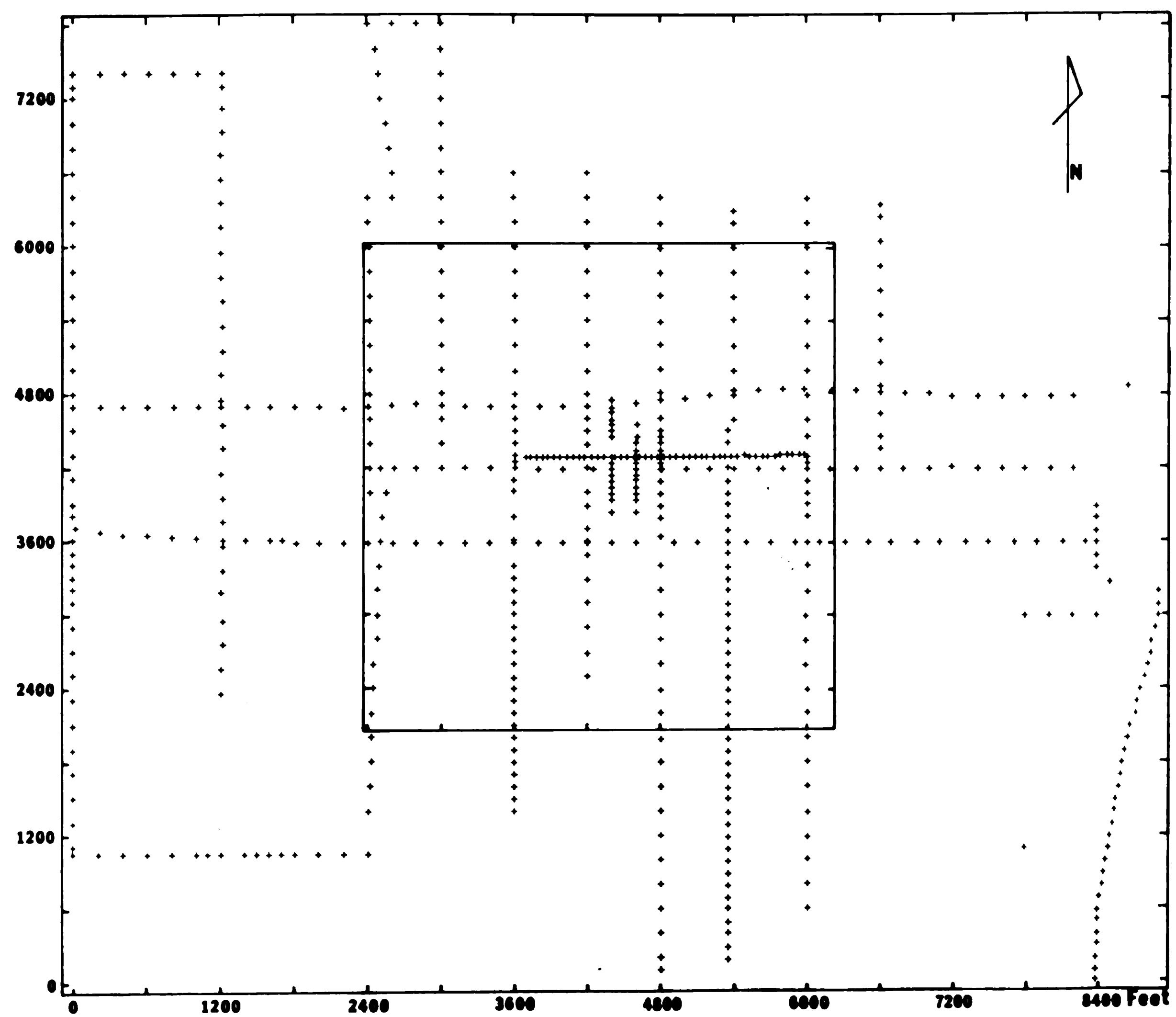

Figure 6. Magnetic survey grid.

Oriented blocks were collected from nine sample sites (Figure 1). Samples were reoriented in the lab and cores 2.54 cm in diameter were drilled for analysis. Susceptibilities of each sample were measured with a Minnetech Magnetic Susceptibility Bridge (Model MS-3). Four to six cores from each block were later analyzed at the University of Michigan's Paleomagnetic Laboratory. Stepwise thermal and a.c. demagnetizations were performed to remove the soft components of the natural remanent magnetization (NRM), and to determine the general character and stability of the remanent magnetization. A.C. demagnetization was performed with a Schonstedt A.C. Demagnetizer (Model GSD-1). During demagnetization the orientation and intensity of the remanent magnetization were measured, between steps, with a Shonstedt Spinner Magnetometer (Model SSM-1).

The computer program SHALOCI developed by Shanabrook (1978), with additions by the author to approximate dipping bodies, was used to model the Michigamme Stock. A complete listing and description of the program is given in Appendix A of Shanabrook (1978).

The computer program SURFACE II was used to contour all the computer modeled anomalies and the field anomalies (Sampson, 1978).

MAGNETIC PROPERTIES

Before the computer modeling process was begun, the magnetic properties of the body were analyzed in detail. As mentioned previously, cores from oriented blocks were analyzed to determine: 1) The stability and types of remanent magnetizations present, 2) The orientation and intensity of the characteristic remanent magnetization, 3) The susceptibility, and 4) The koenigsberger ratio (Q value) of the remanent intensity to induced intensity. Thermal and a.c. demagnetizations show the body to possess a variety of magnetic stabilities and magnetizations, with the characteristic remanent magnetization reversed and more intense then the induced magnetization.

Orientation of the Characteristic Remanent Magnetization

The methods of progressive thermal and a.c. demagnetization were used to determine the character and types of magnetizations present in the samples and to clean the samples of weak secondary magnetizations. In effect this was done to sort out unreliable data, and to determine the orientation and intensity of the characteristic remanent magnetization.

Zijderfeld (1967), developed a method of representing progressive demagnetization to identify the direction and intensity of the various magnetizations possessed by a sample. This information is displayed through orthogonal projections (Generally onto the NS and EW planes) of the curve described by the endpoint of the magnetization vector as it undergoes changes during progressive demagnetizations. Through this method secondary magnetizations were eliminated and the orientation and intensity of the characteristic remanent magnetization were determined.

Representative Zijderfeld diagrams of each sample site are shown in Figures 7 and 8. The orientations and intensities, determined by this method, for each sample are listed in Appendix C. The average orientation for each sample site are listed in Table 1.

Thermal and a.c. demagnetization curves, shown in Figure 9, provide a quick overview of the types of magnetizations present at each sample site. Sample sites (C, D&E, 1A, 2A, and 3A) exhibit stable and hard magnetizations, all of which have similar characteristic remanent magnetization directions. Sample sites (A&B, F, G) possess unstable soft magnetizations, which are due to a viscous secondary magnetization. These samples possess high Q values (See Table 3) and exhibit random orientations that deviate from the orientations found in the more stable samples; for this reason these samples were not used in determining the intensity and orientation of the characteristic remanent magnetization. It is assumed that the high Q values are due to lightning strikes which have altered the remanent magnetization (Strangeway, 1965).

Sample sites (D&E) exhibit unique demagnetization curves that indicate a self-reversal process taking place. The intensity of the remanent magnetization initially increases during demagnetization rather than decreases. The same phenomenon is found in paleomagnetic studies of the Lower Keweenawan Baraga Dikes (Graham, 1953; Vincenz and Yaskawa, 1968). Both authors believe this phenomenon to be an example of a self-reversal process, see (Nagata, 1955; Neel, 1955; Blackett, 1956). Graham (1953) attributed the reverse remanent magnetization to a

Figure 7. Zijderfeld Diagrams, Sample Sites (A, B, C, F).

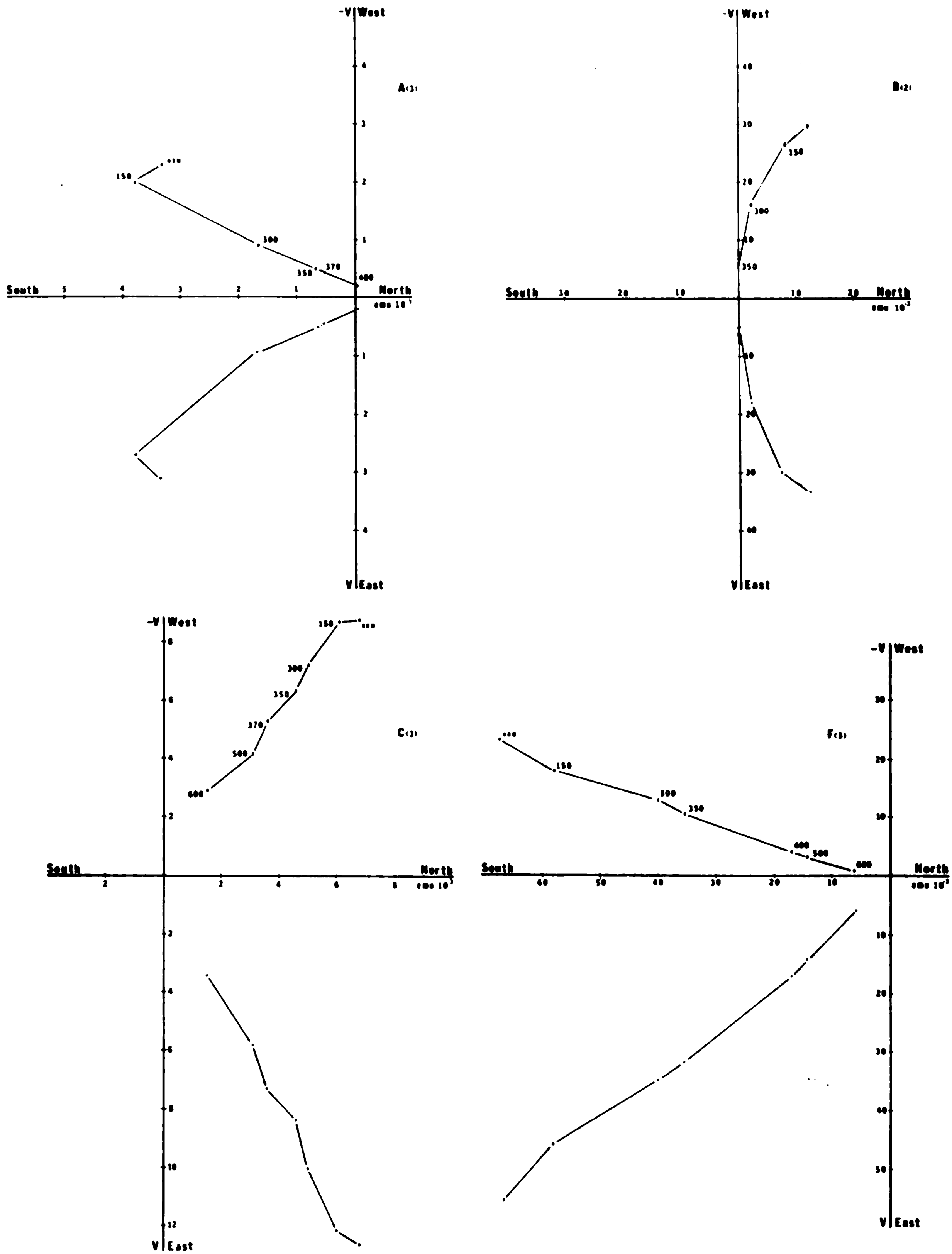
-V West
V East
South
North
A(3)
B(2)
C(3)
F(3)
150
300
350
370
400
500
600

Figure 8. Zijderfeld Diagrams, Sample Sites (D, E, 1A, 2A, 3A).

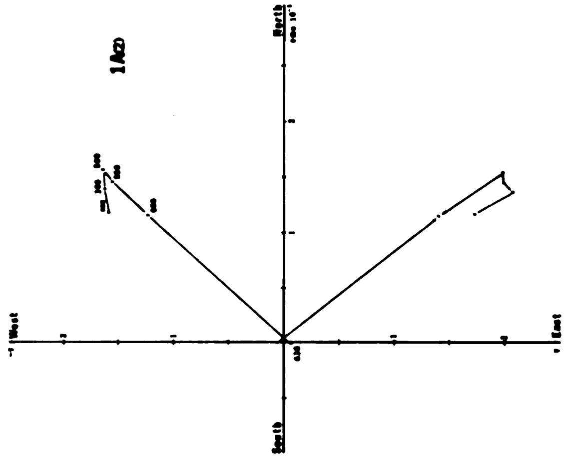
North
South
East
West

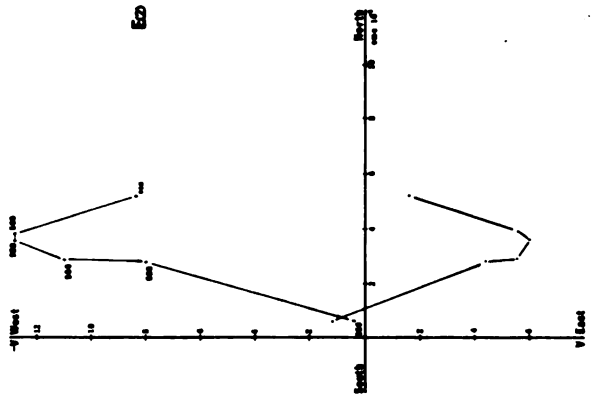
North
South
East
West

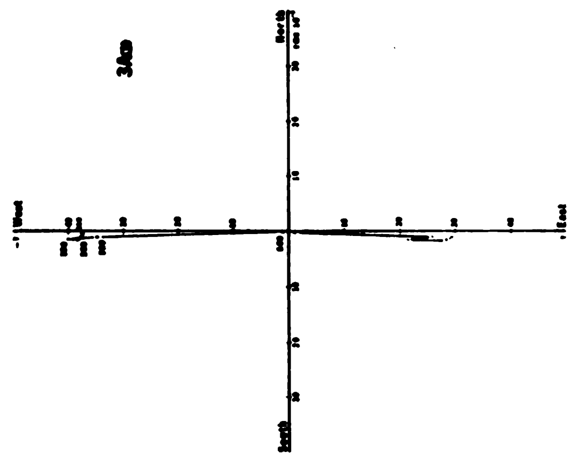
North
South
East
West

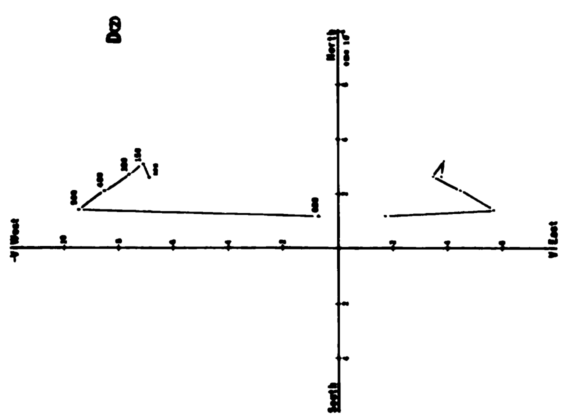
North
South
East
West

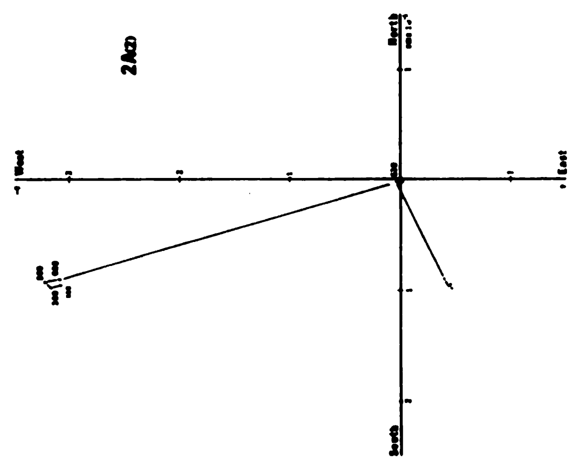
North
South
East
West

Figure 9. Thermal and A.C. Demagnetization Curves.

Table 1. Average Remanent Magnetization Orientation for Each Sample Site.

Sample Site	Ave. NRM Orientation (Not Cleaned)		Ave. Remanent Mag. Orientation (Thermal Clean)		Ave. Remanent Mag. Orientation (A.C. Cleaned)	
	Dec.	Inc.	Dec.	Inc.	Dec.	Inc.
A*	135.8	-31.0	151.1	-26.6	117.0	-30.3
B*	80.5	-40.0	81.2	-39.7	102.7	-42.0
C	64.1	-43.0	62.6	-37.5	66.9	-42.0
D	56.0	-52.0	72.8	-62.9	-----	-----
E	32.0	-57.0	74.4	-56.9	-----	-----
F*	149.0	-28.0	148.8	-24.0	178.8	-23.1
G*	72.6	-54.5	Random		Random	
1A	54.9	-42.0	52.2	-38.9	58.2	-47.6
2A	138.0	-69.0	130.8	-67.4	149.9	-66.9
3A	82.7	-62.0	98.9	-68.5	-----	-----
Average	82.5	-46.8	74.5	-51.4	77.9	-52.1

Characteristic Remanent Magnetization Orientation
(Average of the thermally and A.C. cleaned sites)

Declination = 76.2
Inclination = -51.8

* Eliminated from determining the Characteristic Orientation

self-reversal process of magnetostatic interaction. Vincenz and Yaskawa (1968) considered it more probable that a small antiparallel component of magnetization was formed by a self-reversal process during a reversed geomagnetic field in the Lower Keweenawan. It is believed by the author that a similar process, as described by Vincenz and Yaskawa (1968), has taken place at sample site (D&E). The orientation of the remanent magnetization for sample sites (D&E) were thus included in computing the average orientation of the characteristic remanent magnetization for the body; however the intensities were not included in computing the average remanent magnetization intensity of the body.

A characteristic remanent magnetization orientation of Declination = 76.2 and Inclination = -51.8 was calculated from the thermal and a.c. cleaned data collected at sample sites (C, D&E, 1A, 2A, 3A). Although thermal and a.c. cleaning had various effects on the pole directions, at the individual sample level (Appendix C), cleaning only slightly enhanced the clustering of the average poles of each site (Figure 10). As shown in Table 1, the average thermal pole and average a.c. pole are similar, with both poles diviating little from the NRM pole. The final characteristic pole was determined by averaging the thermal pole and the a.c. pole.

The paleopole position for this characteristic remanent magnetization direction was determined using the method described by McElhinney (1973). Comparison with paleopoles from other Lower Keweenawan Formations (Table 2), shows the pole to be slightly different. When plotted onto the apparent polar wandering track determined by Irving and McGlynn (1976) and age of 1.19 bybp is suggested; compared to an age of 1.13 bybp suggested for other lower Keweenawan Poles. This indicates that the east-west trending reversely

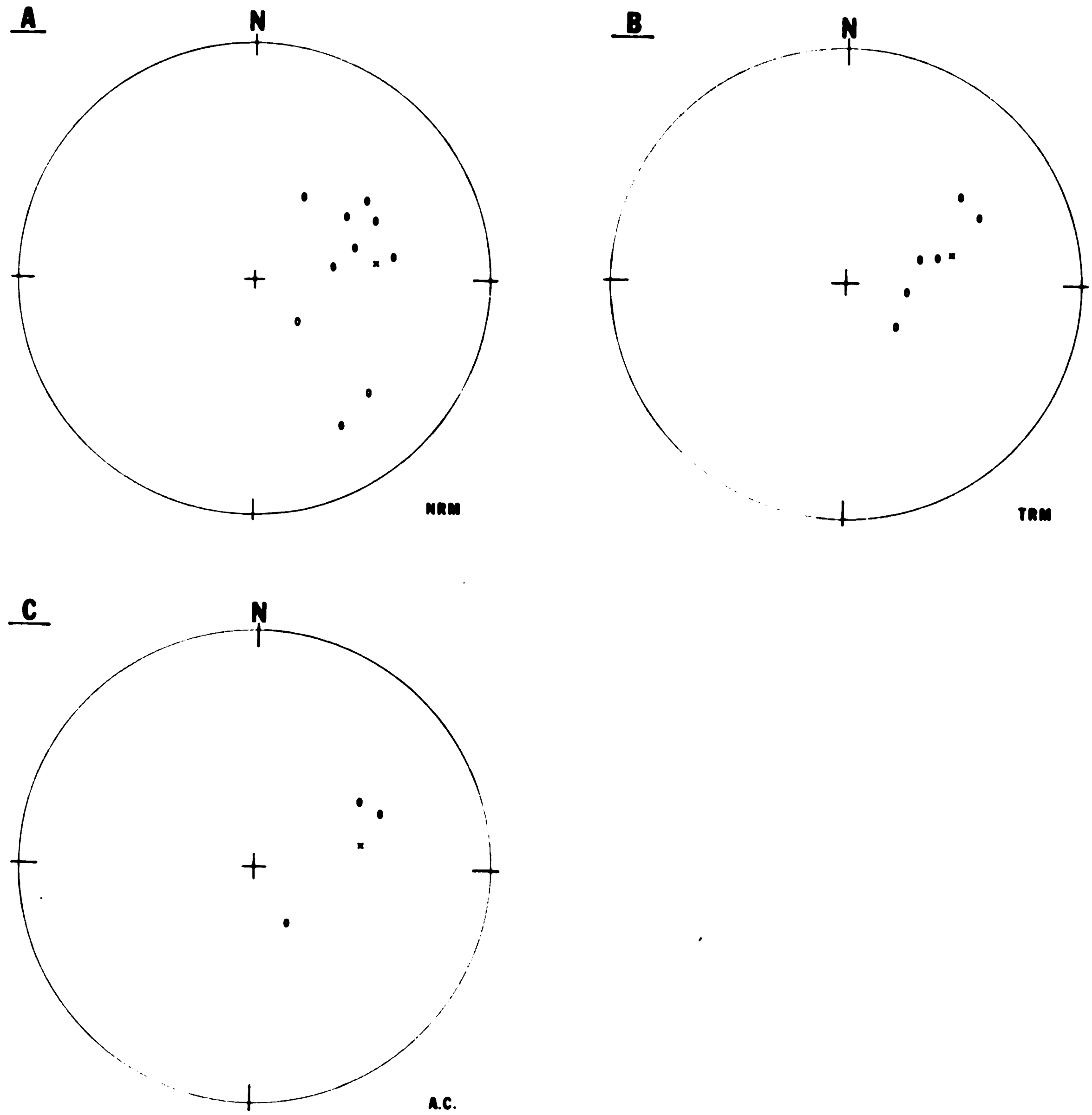

Figure 10. Remanent magnetization declination & inclination stereo plots: A) NRM, B) Thermal cleaned, C) A.C. cleaned.

Table 2. Lower Keweenawan Paleomagnetic Poles.

Area Source	Cleaning	Pole Position	Dec.	Inc.	k
Logan Sills/ Palmer (1970)	A.C.	141.7W, 48.4N	109.0	-71.2	53
Osler Group/ Palmer (1970)		156.7W, 48.9N	117.5	-64.5	24
Grand Portage/ Palmer (1970)		159.8W, 47.0N	116.4	-62.9	30.5
Grand Portage/ Books (1968)		163.0W, 44.5N	117.0	-59.2	
Duluth Gabbro/ Beck (1970)	A.C.	156.5W, 42.5N	91.0	-65.5	44.2
Baraga Dikes/ Graham (1953)		99.5W, 45.0N			
Michigamme Stock/ This Study (1979)		146.2W, 14.7N	76.2	-51.8	

polarized dikes were emplaced before the Keweenawan Lavas and Logan Sills. The ages are also in near agreement with the date of 1.14 bybp given by Chase and Gilmer (1976) for the beginning of rifting.

The Remanent Magnetization Intensity

The resultant measurements of the remanent magnetization intensity, at each sample site (Table 3), show the intensity to vary significantly across the body. The average site intensities vary from a moderate 10.8 x 10^{-5} emu/cm^3 to some unusually high intensities as strong as 8,252. x 10^{-5} emu/cm^3. Remanent intensities of this magnitude are not typical but have also been observed in the Lower Keweenawan, Baraga County, diabase dikes (Vincenz, 1968). As mentioned previously these atypical intensities are assumed to be alteration due to lightning strikes. For this reason the unusually high intensities, samples (A, B, & F), were eliminated from approximations of the bodies average remanent magnetization intensity. Also eliminated were samples (D&E), which exhibit alternations in intensity due to a partial self-reversal mechanism.

The remanent magnetization intensities of the remaining sample sites (C, G, 1A, 2A, 3A) still vary significantly, ranging from 53.9 x 10^{-5} emu/cm^3 to 652.0 x 10^{-5} emu/cm^3, with an average intensty of 322.8 x 10^{-5} emu/cm^3. Due to the the large variation in the intensities, the average intensity of 322.8 x 10^{-5} emu/cm^3 is used as an initial approximation of the body's remanent magnetization.

Susceptibility

The magnetic susceptibility measurements are consistantly weak, ranging from 4.0 x 10^{-5} emu/cm^3 to 30.0 x 10^{-5} emu/cm^3, (Table 3).

Table 3. Average Remanent Magnetization Intensity, Susceptibility, and Q-Ratio for Each Sample Site.

Sample Site	J_R (X 10^{-5})	J_{RC} (X 10^{-5})	k (X 10^{-5})	J_I (X 10^{-5})	Q
1	---	---	8.0	---	---
2	---	---	4.0	---	---
A*	1062.0	767.0	14.0	7.7	99.6
B*	5952.0	4731.0	30.0	16.5	286.7
C	674.0	652.0	9.0	5.0	130.4
D*	10.8	13.4	---	---	---
E*	18.1	23.2	14.0	7.7	3.0
F*	8252.0	8293.0	15.0	8.3	999.2
G	195.0	195.0	10.0	5.5	35.5
1A	348.0	368.0	9.0	5.0	73.6
2A	353.0	345.0	10.0	5.5	62.7
3A	56.4	53.9	4.0	2.2	24.5
Ave.	325.3	322.8	8.4	4.62	65.3

Ave. $Q = J_R/J_I$ 69.9 (Range 25 - 130)

J_R Natural Remanent Magnetization Intensity

J_{RC} Remanent Magnetizatiton Intensity (Cleaned)

k Susceptibility

J_I Induced Magnetization (J_I - kHe)

Q Koenigsberger Ratio (J_R/J_I)

*Eliminated

These remarkably low susceptibilities are similar to those found in Keweenawan acidic intrusives and sediments, and in Precambrian metadiabases and greenstones (Hinze, O'Hara, Secor, and Trow, 1966). Induced magnetic anomalies due to such low susceptibilities are extremely weak.

Koenigsberger Ratio (Q-Ratio)

If the induced and remanent components of magnetization are comparable in intensity, then the Q-ratio (remanent intensity to induced intensity) can be an important tool in magnetic modeling. By holding Q constant and equally increasing or decreasing the remanent and induced components of magnetization, as shown in Figure 11, first order modeling can be done along one specific magnetization axis. In this study the extremely low induced component of magnetization (4.6×10^{-5} emu/cm^3) is negligible compared to the unusually high remanent magnetization (322.8×10^{-5} emu/cm^3). The Q-ratio is very high indicating that the remanent magnetization is dominating the induced magnetization (Table 3). In this case, magnetic modeling is completely dependent on the remanent magnetization.

Summary

The Michigamme Intrusion is ideal for a case magnetic modeling study considering remanent magnetization. The characteristic remanent magnetization orientation is reversed and the remanent magnetization intensity is much larger then the induced magnetization, as indicated by the high Q-ratios. Although variations have been measured in the magnetic properties of the intrusion it is assumed that these variations

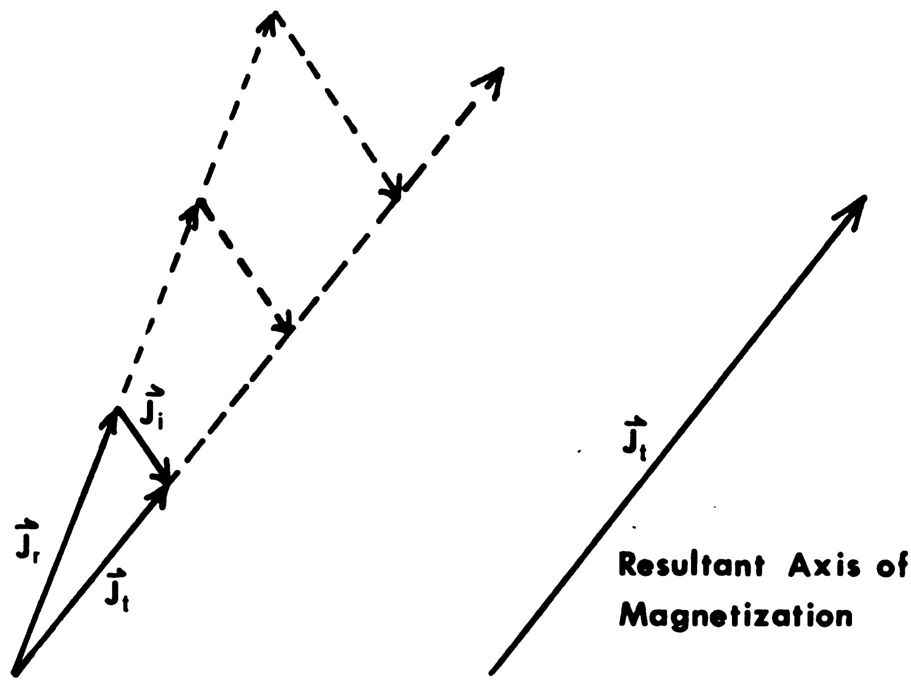

Figure 11. Total magnetization axis.

have been sufficiently filtered out to approximate a magnetic homogeneous body with the following properties;

1) Characteristic remanent magnetization orientation

   Inclination -51.8

   Declination 76.2

2) Remanent magnetization intensity

   Ave. 322.8×10^{-5} emu/cm^3

   Range 53.9×10^{-5} emu/cm^3 - 652.0×10^{-5} emu/cm^3

3) Susceptibility

   $k = 8.4 \times 10^{-5}$ emu/cm^3

4) Q-Ratio

   Ave. 69.9

   Range 25 - 130

MAGNETIC MODELING

The theoretical framework for this study is based upon the magnetic modeling of vertical prism-shaped bodies with arbitrary polarization (Bhattacharryya, 1964). Computer modeling of vertical prism-shaped bodies with arbitrary induced polarization was demonstrated by Whitehill (1973). Shanabrook (1978) expanded Whitehill's computer method to more accurately describe arbitrary polarization as the vector addition of an induced magnetization component and a remanent magnetization component. The modeling program (Shaloci) developed by Shanabrook (1978), with an addition by the author to approximate dipping bodies is used to model the Michigamme Stock.

Theoretical Model

The magnetic field H(x,y,z) at a point P(x,y,z) exterior to a vertical shaped-prism, described in Figure 12, is: (Bhattacharryya, (1964).

The total magnetic intensity of a vertical prism (T).

$$T = I_p \; [LH_x(x,y,z) + MH_y(x,y,z) + NH_z(x,y,z)]$$

$$H_x(x,y.z) = I_p \; [\frac{N}{2} \log(\frac{r+v}{r-v}) + M\log(r+w) + L\tan^{-1} \frac{uv}{u^2+w^2+rw^2}] \; \Big/_{u_o}^{u^1} \Big/_{v_o}^{v^1} \Big/_{w_o}^{w^1}$$

$$H_y(x,y,z) = I_p \; [\frac{N}{2} \log(\frac{r+u}{r-u}) + L\log(r+w) = M\tan^{-1} \frac{uv}{r^2+rw-u^2}] \; \Big/_{u_o}^{u^1} \Big/_{v_o}^{v^1} \Big/_{w_o}^{w^1}$$

$$H_z(x,y,z) = I_p \; [\frac{M}{2} \log(\frac{r+u}{r-u}) + \frac{L}{2}\log(\frac{r+v}{r-v}) - N\tan^{-1} \frac{uv}{rw}] \; \Big/_{u_o}^{u^1} \Big/_{v_o}^{v^1} \Big/_{w_o}^{w^1}$$

Where: I_p = intensity of magnetization of the prism.

(L,M,N) = direction consines $\vec{I}_p$

$r = (u^2 + v^2 = w^2)$

$u_o = x_o - x \qquad u_1 = x_1 - x$

$v_o = y_o - y \qquad v_1 = y_1 - y$

$w_o = z_o - z \qquad w_1 = z_1 - z$

When: $\vec{I}_p$ is due to an <u>induced</u> polarization

$\vec{I}_p = k.\vec{Fe}$

k = the magnetic susceptibility of the prism

$\vec{F}_e$ = the earth's magnetic field

When: $\vec{I}_p$ is due to an <u>induced</u> magnetization component and a <u>remanent</u> magnetization component.

$\vec{I}_p = k\cdot\vec{F}_e + \vec{J}_R$

Where: $\vec{J}_R$ = <u>remanent</u> magnetization of the prism.

$\vec{J}_R = (J_y + J_y + J_z) = (\ J \cos I \cos D\ + J \cos I \sin D + J\ \sin I)$

J = intensity of natural remanent magnetization

I = inclination of the remanent magnetization

D = declination of the remanent magnetization

The <u>vertical magnetic field</u> intensity of a vertical prism (H_z) used in this study:

$$H_z(x,y,z) = I_p \ \left[\frac{M}{2} \log\left(\frac{r+u}{r-u}\right) + \frac{L}{2}\mathrm{Log}\left(\frac{r+v}{r-v}\right) - N\mathrm{Tan}^{-1}\left(\frac{uv}{rw}\right)\right] \Big/_{u_o}^{u^1} \Big/_{v_o}^{v^1} \Big/_{w_o}^{w^1}$$

Where: $\vec{I}_p = k\cdot\vec{F}_e + \vec{J}_R$

A)

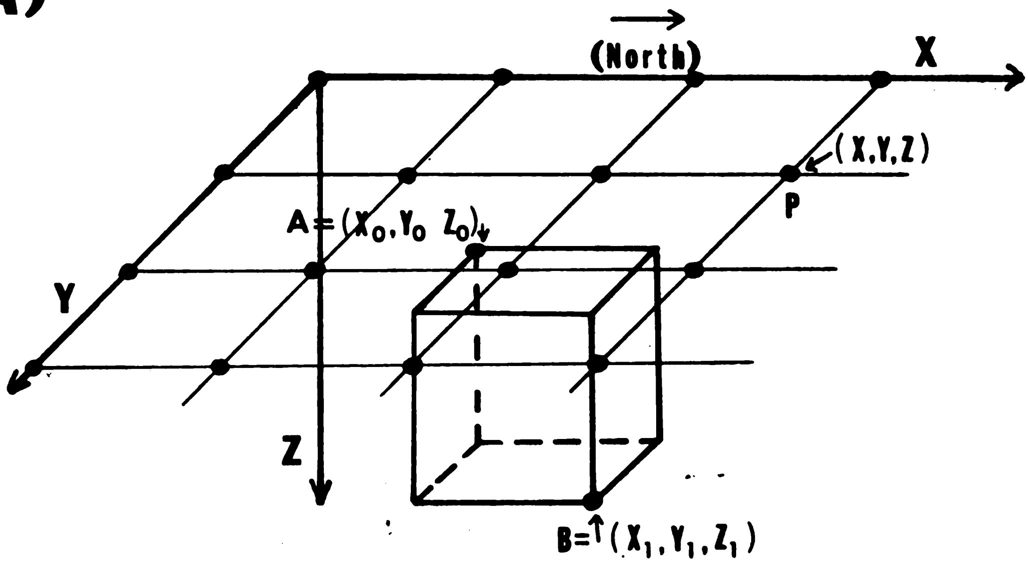

B)

PARAMETERS

PRISM LOCATION

Coordinate Grid Size

Columns(y) 20
Rows(x) 20
Unit One 250 Feet

Cordinate of each Prism

Points $(A_1,B_1)\cdots,(A_N,B_N)$

PRISM MAGNETIC PROPERTIES

Induced Component

Latitude
Longitude
Susceptibility

Remanent Component

Declination
Inclination
Intensity

Figure 12. Computer model: A) Coordinate system, B) Parameters.

Computer Model

The program Shaloci, see Appendix A of Shanabrook (1978), is used to calculate the vertical magnetic field generated by a series of vertical prism-shaped bodies, defined by the parameters shown in Figure 12.

A separate input program for Shaloci was developed by the author to arrange a system of prisms to approximate a dipping cylinder, (See Appendix D). A series of 15 rows of stacked prisms, each row containing 9 prisms inscribed in a circle, are used to define a cylinder (Figure 12a, b). Given any dip and dip direction the rows of prisms are moved an appropriate amount to describe the desired dipping cylinder. Due to a 50 prism input limitation into Shaloci, the stacked prisms are divided into 3 vertical levels each containing 45 prisms. Each level is run through Shaloci separately and the outputs are combined.

The vertical magnetic field output generated by each model is displayed at 400 positions on a 20x20 matrix over the model, Figure 13. The resultant magnetic intensities are then contoured by the program SURFACE II, (See Appendix E for the program commands).

Approximations

By being aware of approximations made in a computer model the error spread produced can be controlled. The reduction of error is a cost factor for the user, errors in a computer model can vertually be eliminated if enough computer memory and time are reserved for compiling the model. Approximations encountered in this study are listed below:

1) Approximation of a dipping cylinder using an assortment of vertical prisms.

Figure 13. Prism Model for Dipping Cylinders.

A)

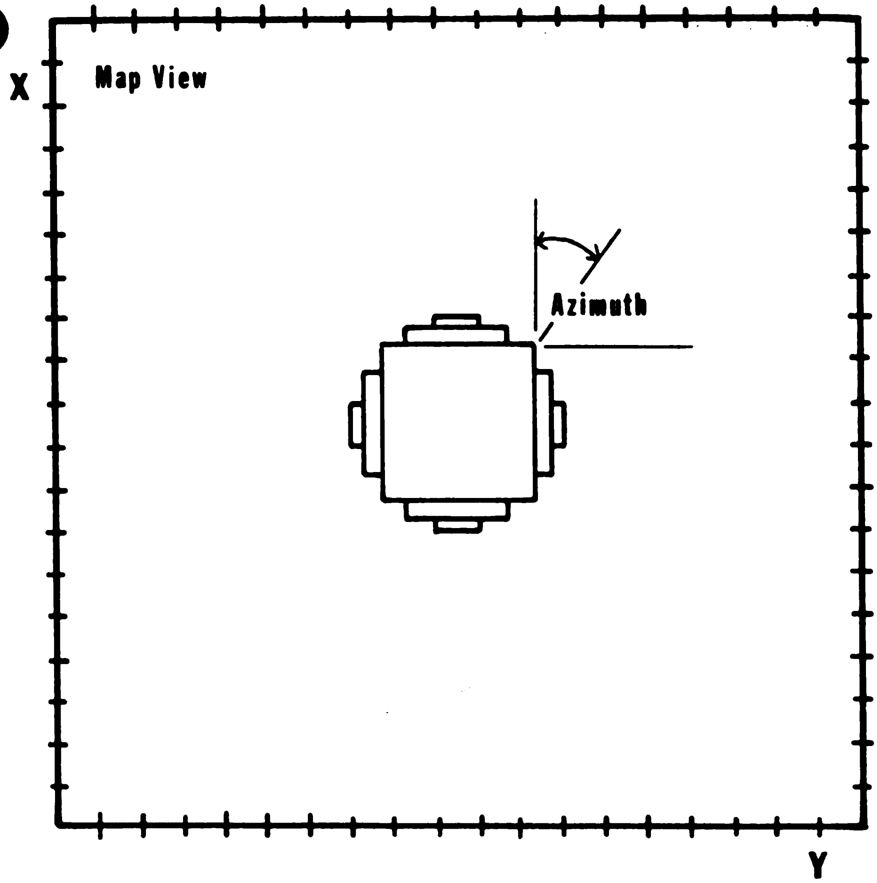
X
Map View
Azimuth
Y

B)

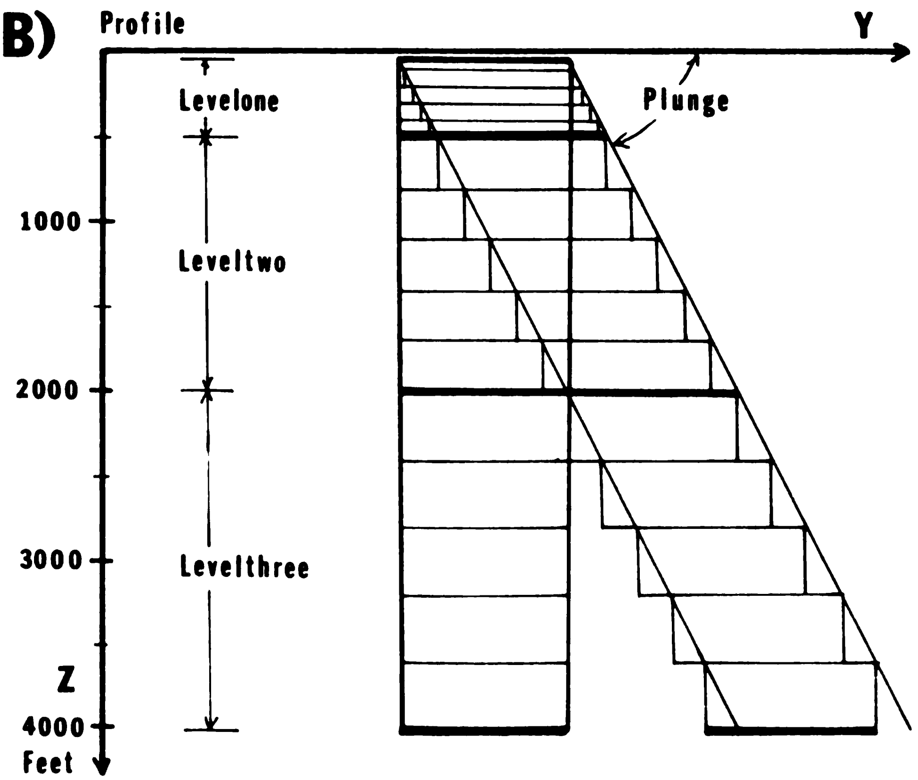
Profile
Y
Levelone
Plunge
1000
Leveltwo
2000
3000
Levelthree
Z
4000
Feet

2) The number of data points (Grid Size) that the magnetic intensity of the anomaly are calculated for over the body.

3) The grid size, type of search pattern, and weighting factor used when regriding the data for contouring.

All of these approximations can be made more efficient by increasing the amount of data put into the model and by requiring more data to be calculated for the output.

It is believed by the author that an appropriate balance between cost and efficiency has been achieved for this study. It is noted here that a certain amount of flexibility is reserved for the final interpretations of the models.

MICHIGAMME STOCK

The Michigamme intrusion was selected to show the importance of remanent magnetization in magnetic interpretations, and to exhibit how easily these interpretations can be performed with a computer, for the following reasons:

1) The intrusion was believed to possess a reverse-remanent magnetization component, which could be confirmed by analyzing samples exposed at the surface.
2) The geometric structure of a stock can easily be modeled by a computer.

Analysis of the magnetic properties of the stock (Chapter 2) have shown that the remanent magnetization is completely dominant, as indicated by the unusually intense remanent magnetization and extremely weak susceptibility (Table 3). It has also been shown that the remanent magnetization is reversed (Table 2). Since the body is dominated by an unusually high remanent magnetization and the field is not parallel to the earth's present field, it is not possible to mistakenly model the anomaly using the susceptibility method. It is concluded that there is a unique anomaly for this structure that is totally dependent upon the intensity and orientation of the remanent magnetization.

Sufficient evidence indicates that the body is a stock (Klasner, 1973) however it is not known in what direction the stock is dipping. Using the remanent magnetization intensity and orientation determined in Chapter 2, modeling of the stock was performed to decern which way the body dips. To demonstrate how this modeling can be performed easily by a computer, the magnetic anomalies due to various dipping stock directions were determined by the computer method previously outlined (Chapter 3). To determine the most appropriate model of the intrusion the computer modeled anomalies were compared to the ground magnetic survey anomaly of the Michigamme Stock (Figure 5).

Two sets of models for the different dipping stocks were performed using the remanent magnetization orientation expected for a Lower Keweenawan Formation (Table 3) and the remanent magnetization orientation measured (Table 1). Because the measured remanent magnetization orientation varied from the orientation expected for a Lower Keweenawan Formation, both sets of models were performed to test the best possible fit for the observed ground magnetic survey anomaly for the Michigamme Stock (Figure 5).

The geologic and geophysical parameters used for the models are outlined in Table 4.

Computer Models of the Michigamme Stock

Models of vertical stocks with varying remanent magnetic intensities were first done to determine the best approximation for the remanent magnetization intensity of the Michigamme Stock. This was done by comparing the maximum and minimum amplitudes of the model anomalies to the amplitudes of the observed anomaly (Figure 5), until the best match was found. A remanent intensity of 150. $\times 10^{-5}$ emu/cm^3, well within the range of intensities measured for the intrusion (Table 3), was found to be the best approximation for the remanent magnetization intensity of the Michigamme Stock. This intensity is used for the following models.

Table 4. Geologic and Geophysical Parameter Values Used in Computer Models I & II.

Geology		
Geometry (Stock)		Klasner
Diameter	1000'	
Depth. to Bottom	4000'	
Dip (?)	67.0°	
Geophysics		
(Induced Magentization Component)		
Orientation (determined from Earth's magnetic Field)		
Latitude	46.5	Topo. Map
Longitude	88.0	
Intensity		
Susceptibility	$k = 8.4 \times 10^{-5}$ emu/cm^3	This Study
(Remanent Magnetization Component)		
Model I		
Orientation		From Lower Keweenawan Paleopole.
Inclination	I = -65.0	
Declination	D = 100.0	
Model II		
Orientation		This Study
Inclination	I = -51.8	
Declination	D = 76.2	
Intensity (J_r)		This Study
Magnitude		
Range	$53.9 - 652.0 \times 10^{-5}$	
Ave.	322.8×10^{-5} emu/cm^3	
Best Fit Value.	150.0×10^{-5} emu/cm^3	

Comparisons of the computer model anomalies to the observed anomaly of the Michigamme Stock (Figure 5) are based on the following criteria:

1) The spatial orientation of the maximum amplitude to the minimum amplitude.
2) Visual comparison of the maximum and minimum amplitudes of the anomalies.
3) Visual comparison of profile curves through the maximum and minimum amplitudes.

The first set of models (Model I), using the remanent magnetization orientation expected for the Lower Keweenawan Formation, are shown in Figures 14 & 15. Model I A, B, C and D (Figure 14) respectively represent a stock dipping 70 degrees to the north, east, south, and west. Comparison of the spatial orientation of the maximum and minimum amplitude show Model IA, of a stock dipping to the north, to be the only model that spatially fits the observed anomaly for the Michigamme Stock (Figure 5). However comparison of the maximum and minimum amplitudes show the maximum amplitude to be less then needed for a good fit. Model I E, F, and G (Figure 15) respectively represent a stock dipping N20E, 70, 50, and 30 degrees. By decreasing the amount of dip toward the north a better match of the maximum amplitude is observed. Profile comparisons (Figure 18A) also show a better curve fit for a stock gently dipping to the north.

The second set of Models (Model II), using the remanent magnetization measured in this study (Table 1), are shown in Figures 16 & 17. Model II A, B, C, and D (Figure 16) respectively represent a stock dipping 70 degrees to the north, east, south, and west. Comparison of the spatial orientation of the maximum and minimum amplitudes show Models II A, B, and D, of a stock dipping to the north,

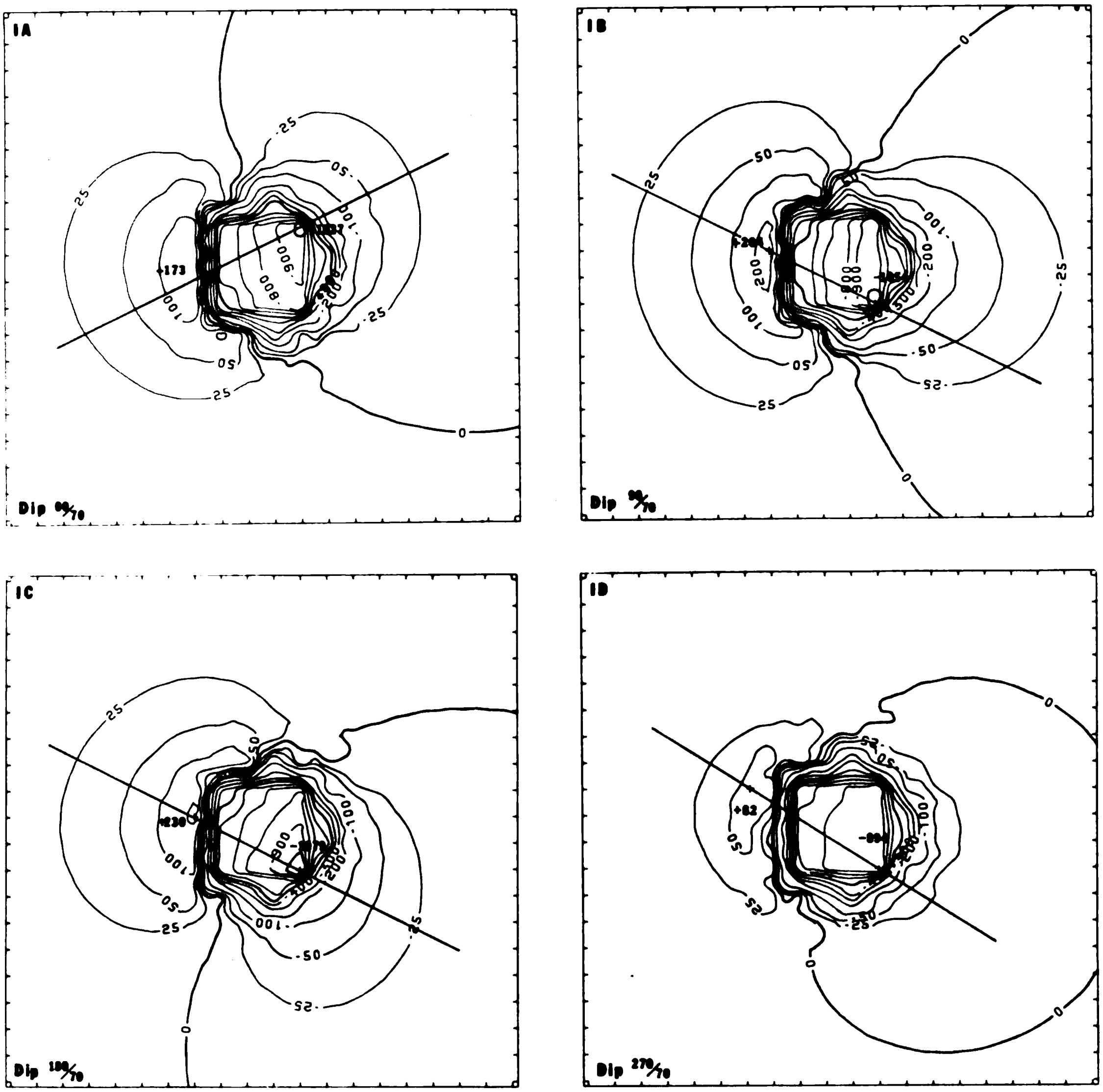

Figure 14. Model I. For a cylinder dipping 70 degrees in the: A) North direction, B) East direction, C) South direction, and D) West direction.

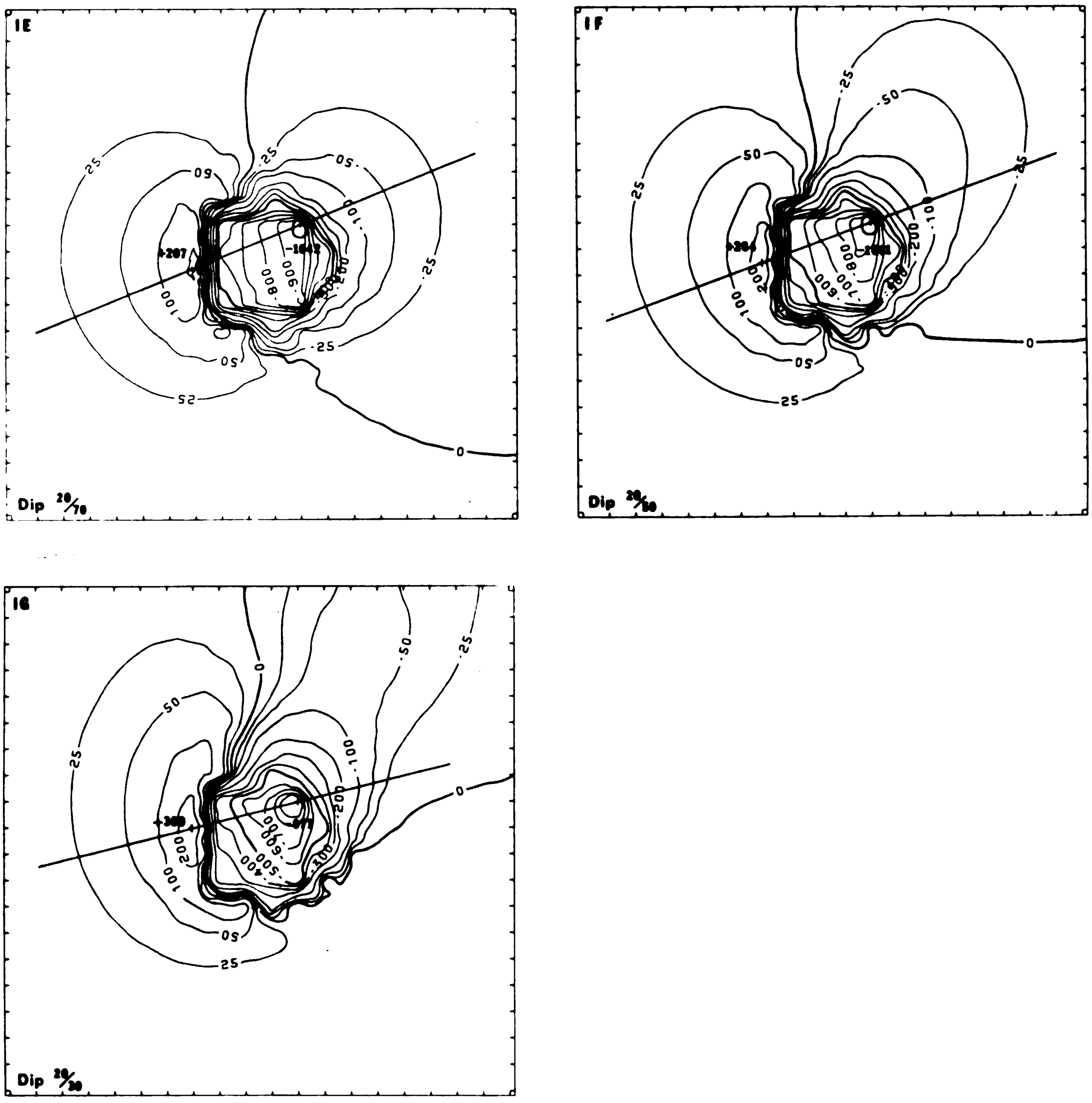

Figure 15. Model I. For a cylinder dipping in the N20E direction: E) 70 dip, F) 50 dip, and G) 30 dip.

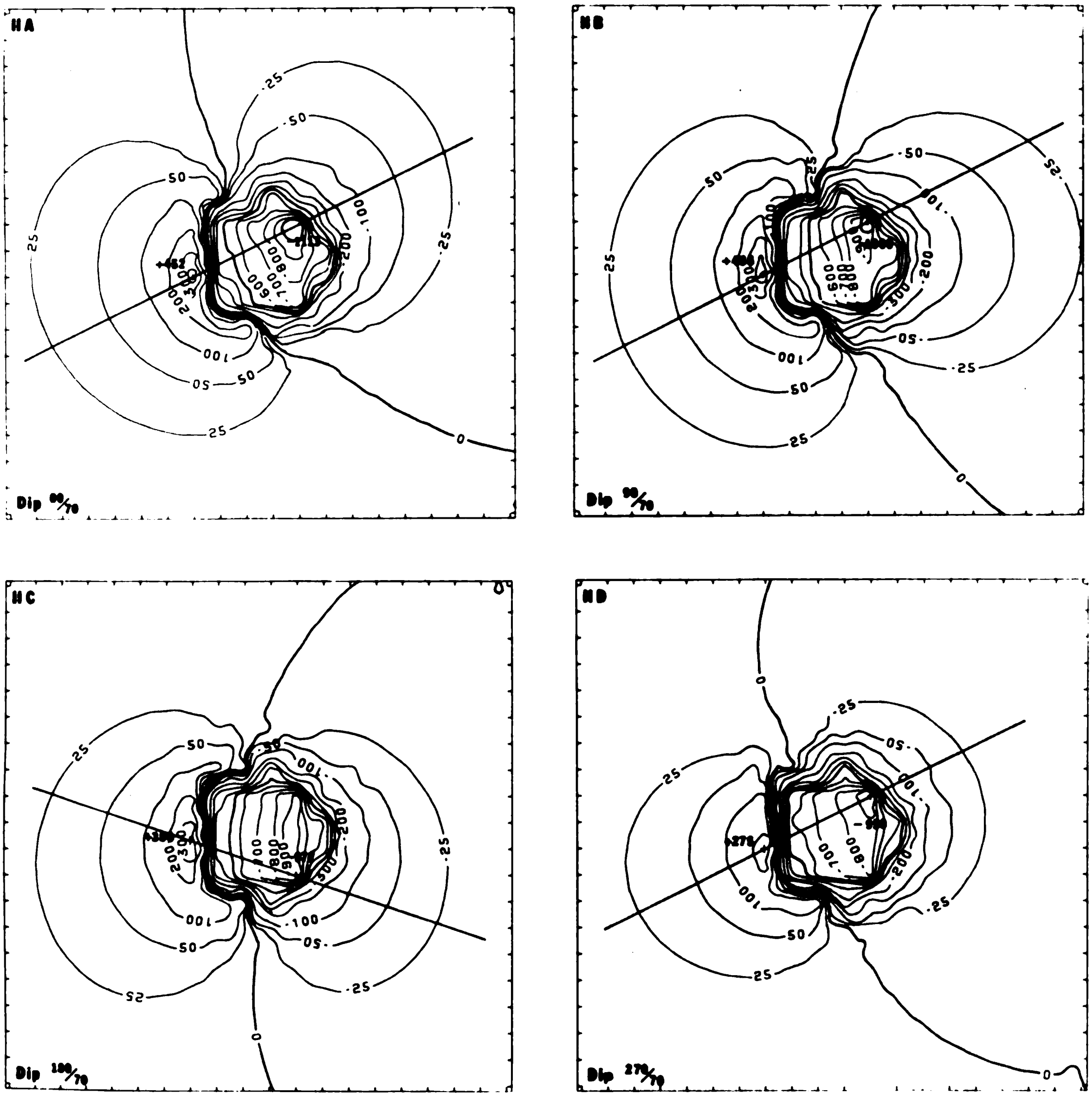

Figure 16. Model II. For a cylinder dipping 70 degrees in the: A) North direction, B) East direction, C) South direction, and D) West direction.

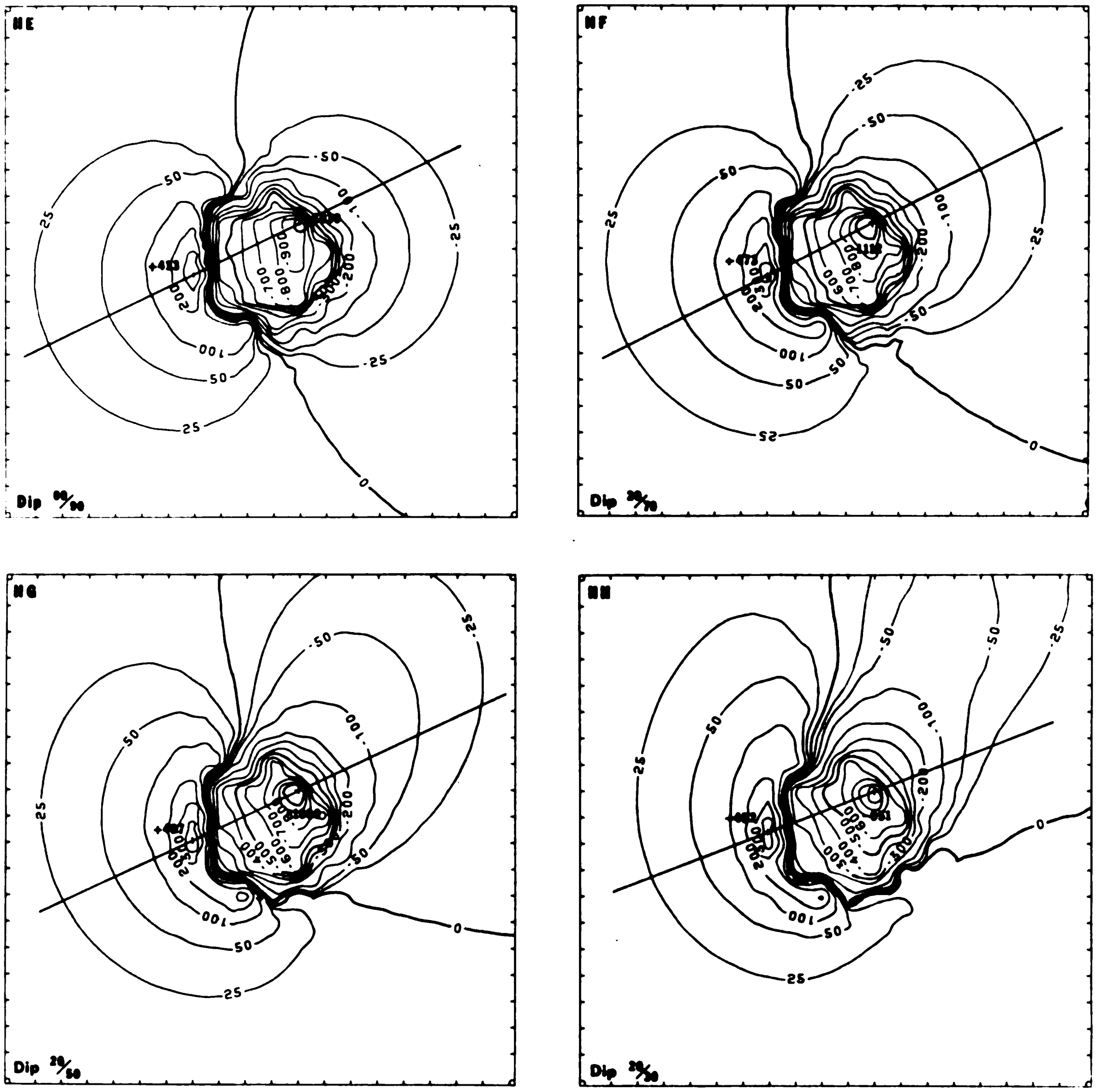

Figure 17. Model II. For a cylinder dipping in the N20E direction: E) 90 dip, F) 70 dip, G) 50 dip, and H) 30 dip.

Figure 18. Model I & II Profiles.
A) Model I Profiles: For a cylinder dipping in the N20°E direction 70°, 50°, and 30°.
B) Model II Profiles: For a cylinder dipping in the N20°E direction 90°, 70°, 50° and 30°.

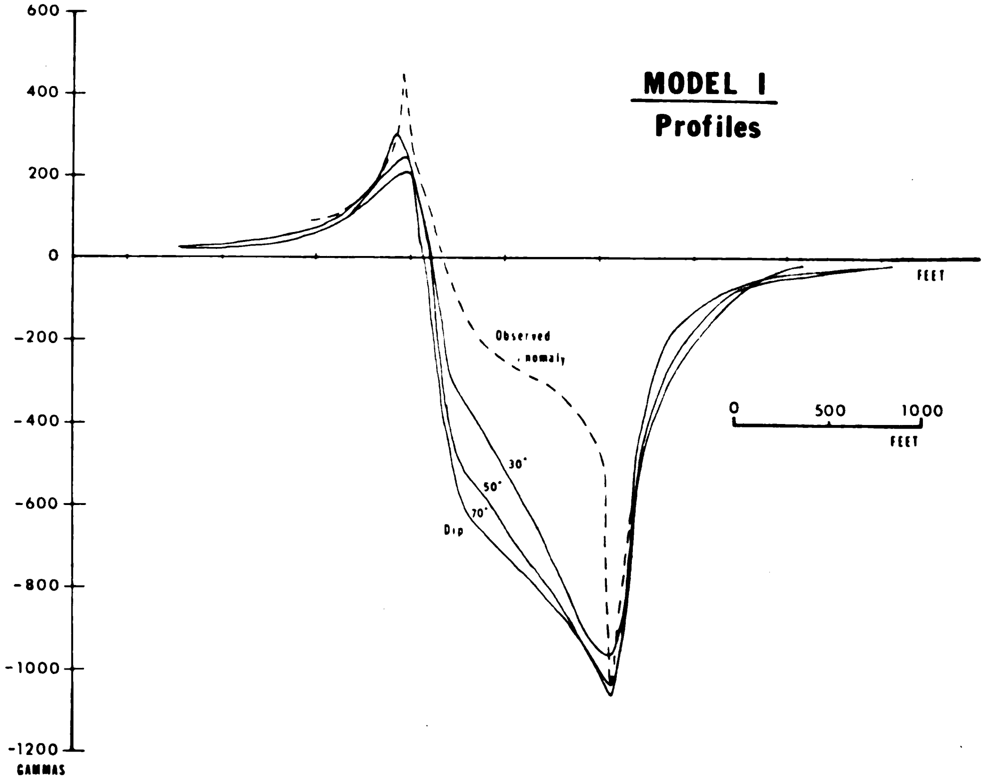
MODEL I
Profiles
600
400
200
0
-200
-400
-600
-800
-1000
-1200
GAMMAS
FEET
Observed
Anomaly
30°
50°
70°
Dip
0
500
1000
FEET

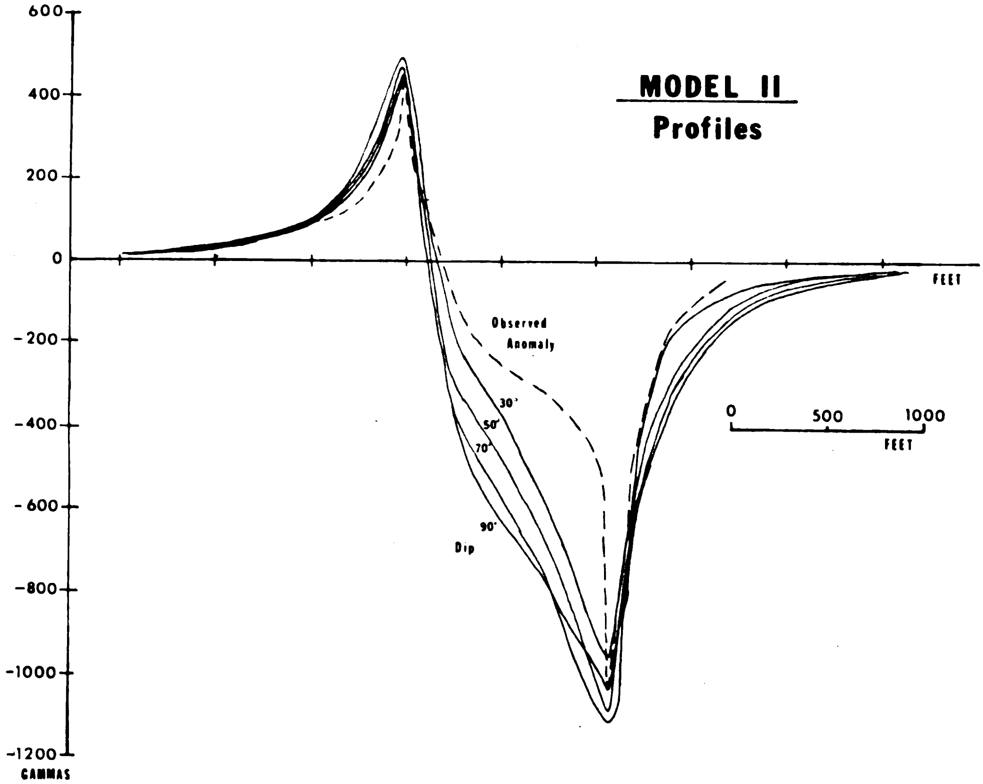
MODEL II
Profiles
600
400
200
0
-200
-400
-600
-800
-1000
-1200
GAMMAS
FEET
Observed
Anomaly
30°
50°
70°
90°
Dip
0
500
1000
FEET

east, and west, to all spatially match the observed anomaly for the Michigamme Stock (Figure 5). In this set of models a better comparison of maximum and minimum amplitudes is observed; with the closest match for a stock dipping to the north. Models II E, F, G, and H (Figure 17) respectively represent a stock dipping N20E, 90, 70, 50, and 30 degrees. The best match of maximum and minimum amplitudes is observed for the vertical stock. However, profile comparisons (Figure 18B) show a better curve fit for a gently dipping stock.

Discussion of Results

The best set of models for the Michigamme intrusion are observed for those models using the remanent magnetization orientation measured in the study (Table 3). the spatial orientation of the maximum and minimum amplitudes and the match of the amplitude magnetudes indicate that Model II E (Figure 17E), for a vertical stock, to be the best match to the observed anomaly for the Michigamme Intrusion (Figure 5). Variations observed in the profile shapes (Figure 18) are assumed to be due to an incorrect initial aproximation that the Michigamme Intrusion is a perfect cylindrical stock. Approximations encountered in the computer modeling require flexibility in the final interpretation, as discussed in Chapter 3. It is more appropriate to interpret the intrusion as being a stock that is vertical or steeply dipping in the northern direction. This is in agreement with the predictions of Klasner (1973), as seen in the cross section view shown in Figure 1.

Even though the best models were achieved using the remanent magnetization orientation measured in the study, first hand approximations using the expected remanent magnetization orientation for the Lower Keweenawan would have sufficed to initially model the stock.

CONCLUSION

It has been shown in this study that remanent magnetization can be a significant factor in the total magnetization of a body, and that magnetic modeling of these bodies can be performed easily with a computer. In the case of the Michigamme Intrusion it was found that the remanent magnetization was completely dominant over the induced magnetization, and that the remanent field was reversed compared to the earth's present field. In this particular case it is not possible to mistakenly model the body using the susceptibility method alone. The magnetic anomaly associated with the Michigamme Intrusion is completely due to a remanent magnetization, which was easily modeled using the computer method outlined in Chapter 2.

It was also shown that a detailed study of the bodies magnetic properties is not completely necessary to model the body, if enough geologic and geophysical information is available for the study area. In the case of the Michigamme Intrusion, magnetic modeling could have been done to decern the structure of the body even if the body were buried, for the following reasons.

1) The spatial orientation of the maximum and minimum amplitudes for the magnetic anomaly deviate from the orientation expected at that latitude and logitude; thus indicating a remanent magnetization component.

2) The magnitude of the minimum negative amplitude is larger then the maximum positive amplitude, indicating a large reverse-remanent magnetization intensity.

3) The observed anomaly is magnetically associated with east-west trending reversely polarized dikes of Lower-Keweenawan age, for which paleopole information is available.

4) The susceptibilities for various rock types in the area are available.

With the information above, magnetic modeling can be performed until the best combination of remanent magnetization and susceptibility is found. If the susceptibility is known, as in this case, modeling of the body was shown to be sufficient by adjusting the remanent magnetization intensity and using the remanent magnetization orientation expected for a Lower Keweenawan Formation.

Although it may not be necessary to perform a detailed field study of the body in question, it is always desirable to obtain the maximum amount of hard data possible to create the best model for the given situation.

APPENDICES

APPENDIX A

Whole Rock Analyses, and Trace and Rare-Earth Element Concentrations (PPM)

Whole Rock Analyses

Sample No.	SiO_2	Al_2O_3	Fe_2O_3	FeO	MgO	CaO	Na_2O	K_2O	LOI	TiO_2	P_2O_5	MnO	Total
ZPK-1 (D4E)	51.32	13.52	2.36	11.05	3.98	7.11	2.37	1.69	2.86	2.47	.30	.18	99.21
ZPK-2 (D4E)	51.91	13.42	2.83	10.72	3.56	6.57	2.92	1.91	3.39	2.59	.33	.17	100.32
LM-2 (F)	50.08	13.89	2.74	11.44	4.06	7.61	2.38	1.41	2.74	2.65	.24	.16	99.40

Trace and Rare-Earth Element Concentrations (PPM).

Sample No.	Ni	Cr	Zn	Cu	Mn	Co	Cr[1]	La	Ce	Sm	Eu	Yb	Lu	La[2]	Sm[2]
ZPK-1 (D4E)	1332	0	120	95	0	45	52	24.8	44	7.28	2.25	1.91	.36	21.6	7.38
ZPK-2 (D4E)	1292	0	121	95	0	43	32	24.8	48	7.74	2.41	3.34	.56	21.5	8.13
LM-2 (F)	1270	0	110	97	0	45	66	13.5	40	6.30	2.13	1.49	.67	21.3	6.66

[1]CR Determined by X-Ray Fluorescence.

[2]La and Sm Analyses with Liquid Standards.

Morris (78).

APPENDIX B

Corrected Vertical Magnetic Intensity Data

Corrected vertical magnetic intensity survey data.

#	LINE #	X	Y	Z	#	LINE #	X	Y	Z
1	A01	4800.0	4600.0	-310.0	31	C11	6000.0	6385.0	4100.0
2	A02	4800.0	4810.0	-130.0	32	D01	6600.0	4350.0	-140.0
3	A03	4800.0	5000.0	-40.0	33	D02	6600.0	4450.0	-70.0
4	A04	4800.0	5200.0	-25.0	34	D03	6600.0	4635.0	-80.0
5	A05	4800.0	5385.0	70.0	35	D04	6600.0	4860.0	-40.0
6	A06	4800.0	5600.0	230.0	36	D05	6600.0	5050.0	0.0
7	A07	4800.0	5785.0	410.0	37	D06	6600.0	5235.0	90.0
8	A08	4800.0	5985.0	770.0	38	D07	6600.0	5435.0	160.0
9	A09	4800.0	6185.0	1725.0	39	D08	6600.0	5635.0	250.0
10	A10	4800.0	6400.0	3550.0	40	D09	6600.0	5835.0	320.0
11	B01	5400.0	6285.0	1325.0	41	D10	6600.0	6035.0	550.0
12	B02	5400.0	6185.0	3000.0	42	D11	6600.0	6235.0	1200.0
13	B03	5400.0	5985.0	825.0	43	D12	6600.0	6335.0	3000.0
14	B04	5400.0	5785.0	470.0	44	E01	4200.0	4000.0	-250.0
15	B05	5400.0	5585.0	290.0	45	E02	4200.0	4200.0	-210.0
16	B06	5400.0	5400.0	130.0	46	E03	4200.0	4385.0	-230.0
17	B07	5400.0	5185.0	40.0	47	E04	4200.0	4500.0	-180.0
18	B08	5400.0	4985.0	-30.0	48	E05	4200.0	4600.0	-200.0
19	B09	5400.0	4785.0	-90.0	49	E06	4200.0	4800.0	-150.0
20	B10	5400.0	4585.0	-150.0	50	E07	4200.0	4985.0	-100.0
21	C01	6000.0	4450.0	-230.0	51	E08	4200.0	5200.0	-30.0
22	C02	6000.0	4585.0	16.0	52	E09	4200.0	5400.0	40.0
23	C03	6000.0	4785.0	-34.0	53	E10	4200.0	5600.0	200.0
24	C04	6000.0	4985.0	-19.0	54	E11	4200.0	5800.0	420.0
25	C05	6000.0	5185.0	47.0	55	E12	4200.0	6000.0	730.0
26	C06	6000.0	5385.0	130.0	56	E13	4200.0	6200.0	1000.0
27	C07	6000.0	5585.0	268.0	57	E14	4200.0	6400.0	1200.0
28	C08	6000.0	5785.0	439.0	58	E15	4200.0	6600.0	2325.0
29	C09	6000.0	5985.0	770.0	59	F01	3600.0	6600.0	2250.0
30	C10	6000.0	6185.0	4687.0	60	F02	3600.0	6400.0	1350.0

Corrected vertical magnetic intensity survey data.

#	LINE #	X	Y	Z	#	LINE #	X	Y	Z
61	F03	3610.0	6200.0	820.0	91	G17	5200.0	4785.0	-106.0
62	F04	3610.0	6000.0	480.0	92	G18	5000.0	4760.0	-86.0
63	F05	3610.0	5800.0	260.0	93	G19	4800.0	4750.0	-97.0
64	F06	3610.0	5600.0	90.0	94	G20	4600.0	4725.0	-117.0
65	F07	3610.0	5400.0	-10.0	95	G21	4200.0	4700.0	-158.0
66	F08	3610.0	5200.0	-100.0	96	G22	4000.0	4700.0	-158.0
67	F09	3610.0	4985.0	-160.0	97	G23	3810.0	4700.0	-178.0
68	F10	3610.0	4800.0	-200.0	98	G24	3600.0	4700.0	-208.0
69	F11	3610.0	4600.0	-220.0	99	G25	3410.0	4700.0	-208.0
70	F12	3610.0	4500.0	-220.0	100	G26	3200.0	4700.0	-198.0
71	F13	3610.0	4400.0	-230.0	101	G27	3010.0	4710.0	-208.0
72	F14	3610.0	4300.0	-320.0	102	G28	2800.0	4725.0	-229.0
73	F15	3610.0	4250.0	-140.0	103	G29	2600.0	4710.0	-229.0
74	F16	3610.0	4200.0	-110.0	104	G30	2410.0	4700.0	-249.0
75	G01	8635.0	4860.0	140.0	105	G31	2210.0	4685.0	-249.0
76	G02	8185.0	4775.0	106.0	106	G32	2010.0	4700.0	-250.0
77	G03	8000.0	4775.0	86.0	107	G33	1810.0	4700.0	-250.0
78	G04	7785.0	4775.0	66.0	108	G34	1610.0	4700.0	-270.0
79	G05	7600.0	4775.0	25.0	109	G35	1425.0	4700.0	-290.0
80	G06	7400.0	4775.0	25.0	110	G36	1210.0	4700.0	-300.0
81	G07	7185.0	4775.0	-5.0	111	G37	1025.0	4700.0	-300.0
82	G08	7000.0	4800.0	-5.0	112	G38	825.0	4700.0	-310.0
83	G09	6800.0	4800.0	-40.0	113	G39	610.0	4700.0	-301.0
84	G10	6600.0	4810.0	-45.0	114	G40	410.0	4700.0	-301.0
85	G11	6400.0	4825.0	-35.0	115	G41	225.0	4700.0	-291.0
86	G12	6200.0	4825.0	-26.0	116	G42	0.0	4700.0	-331.0
87	G13	5975.0	4835.0	-54.0	117	H01	0.0	4510.0	-312.0
88	G14	5800.0	4835.0	-76.0	118	H02	0.0	4300.0	-322.0
89	G15	5600.0	4825.0	-96.0	119	H03	0.0	4110.0	-292.0
90	G16	5400.0	4825.0	-116.0	120	H04	0.0	3900.0	-292.0

Corrected vertical magnetic intensity survey data.

#	LINE #	X	Y	Z	#	LINE #	X	Y	Z
121	H05	0.0	3810.0	-267.0	151	I14	3600.0	2485.0	140.0
122	H06	0.0	3610.0	-252.0	152	I15	3600.0	2400.0	161.0
123	H07	0.0	3500.0	-252.0	153	I16	3600.0	2300.0	201.0
124	H08	0.0	3410.0	-233.0	154	I17	3600.0	2200.0	251.0
125	H09	0.0	3300.0	-173.0	155	I18	3600.0	2100.0	102.0
126	H10	0.0	3210.0	-233.0	156	I19	3600.0	2000.0	298.0
127	H11	0.0	3100.0	-193.0	157	I20	3600.0	1900.0	342.0
128	H12	0.0	2900.0	-133.0	158	I21	3600.0	1800.0	252.0
129	H13	0.0	2700.0	-194.0	159	I22	3600.0	1700.0	393.0
130	H14	0.0	2510.0	-64.0	160	I23	3600.0	1600.0	514.0
131	H15	0.0	2310.0	-64.0	161	I24	3600.0	1500.0	1143.0
132	H16	0.0	2100.0	-64.0	162	I25	3600.0	1400.0	543.0
133	H17	0.0	1900.0	-24.0	163	J01	5350.0	4500.0	-164.0
134	H18	0.0	1710.0	-15.0	164	J02	5350.0	4400.0	-243.0
135	H19	0.0	1510.0	26.0	165	J03	5350.0	4200.0	-189.0
136	H20	0.0	1300.0	145.0	166	J04	5350.0	4085.0	-248.0
137	H21	0.0	1110.0	545.0	167	J05	5350.0	3985.0	-165.0
138	I01	3600.0	4100.0	-87.0	168	J06	5350.0	3900.0	-254.0
139	I02	3600.0	4010.0	-85.0	169	J07	5350.0	3800.0	-201.0
140	I03	3600.0	3800.0	-45.0	170	J08	5350.0	3685.0	-240.0
141	I04	3600.0	3610.0	-24.0	171	J09	5350.0	3585.0	-230.0
142	I05	3600.0	3400.0	385.0	172	J10	5350.0	3500.0	-206.0
143	I06	3600.0	3300.0	285.0	173	J11	5350.0	3385.0	-165.0
144	I07	3600.0	3200.0	18.0	174	J12	5350.0	3285.0	-162.0
145	I08	3600.0	3100.0	28.0	175	J13	5350.0	3200.0	-121.0
146	I09	3600.0	3010.0	59.0	176	J14	5350.0	3085.0	-120.0
147	I10	3600.0	2900.0	-10.0	177	J15	5350.0	3000.0	-99.0
148	I11	3600.0	2800.0	30.0	178	J16	5350.0	2885.0	-117.0
149	I12	3600.0	2700.0	50.0	179	J17	5350.0	2785.0	-76.0
150	I13	3600.0	2600.0	140.0	180	J18	5350.0	2685.0	5.0

Corrected vertical magnetic intensity survey data.

#	LINE #	X	Y	Z	#	LINE #	X	Y	Z
181	J19	5350.0	2585.0	-73.0	211	K06	3010.0	5200.0	-236.0
182	J20	5350.0	2485.0	28.0	212	K07	3010.0	5400.0	-184.0
183	J21	5350.0	2385.0	109.0	213	K08	3010.0	5600.0	-94.0
184	J22	5350.0	2285.0	11.0	214	K09	3010.0	5800.0	27.0
185	J23	5350.0	2185.0	14.0	215	K10	3010.0	6000.0	134.0
186	J24	5350.0	2085.0	74.0	216	K11	3010.0	6200.0	308.0
187	J25	5350.0	1985.0	82.0	217	K12	3010.0	6400.0	528.0
188	J26	5350.0	1885.0	118.0	218	K13	3010.0	6610.0	719.0
189	J27	5350.0	1785.0	139.0	219	K14	3010.0	6800.0	860.0
190	J28	5350.0	1685.0	193.0	220	K15	3010.0	7000.0	931.0
191	J29	5350.0	1585.0	243.0	221	K16	3010.0	7200.0	1072.0
192	J30	5350.0	1500.0	304.0	222	K17	3010.0	7400.0	1253.0
193	J31	5350.0	1385.0	376.0	223	K18	3010.0	7600.0	2404.0
194	J32	5350.0	1285.0	460.0	224	K19	3010.0	7810.0	2500.0
195	J33	5350.0	1185.0	531.0	225	K20	2810.0	7810.0	8000.0
196	J34	5350.0	1085.0	652.0	226	K21	2610.0	7810.0	30000.0
197	J35	5350.0	985.0	725.0	227	L01	2410.0	7810.0	19000.0
198	J36	5350.0	885.0	816.0	228	L02	2475.0	7600.0	3200.0
199	J37	5350.0	785.0	958.0	229	L03	2500.0	7400.0	1295.0
200	J38	5350.0	685.0	1099.0	230	L04	2510.0	7200.0	821.0
201	J39	5350.0	600.0	1250.0	231	L05	2560.0	7000.0	591.0
202	J40	5350.0	485.0	1611.0	232	L06	2585.0	6800.0	542.0
203	J41	5350.0	400.0	2100.0	233	L07	2610.0	6600.0	478.0
204	J42	5350.0	285.0	3000.0	234	L08	2610.0	6400.0	344.0
205	J43	5350.0	185.0	3600.0	235	L09	2410.0	6400.0	279.0
206	K01	3010.0	4200.0	-132.0	236	L10	2410.0	6200.0	179.0
207	K02	3010.0	4400.0	-228.0	237	L11	2425.0	6000.0	150.0
208	K03	3010.0	4600.0	-228.0	238	L12	2425.0	5800.0	120.0
209	K04	3010.0	4810.0	-237.0	239	L13	2425.0	5600.0	31.0
210	K05	3010.0	5000.0	-256.0	240	L14	2425.0	5400.0	-57.0

Corrected vertical magnetic intensity survey data.

#	LINE #	X	Y	Z	#	LINE #	X	Y	Z
241	L15	2425.0	5200.0	-117.0	271	N14	2000.0	1050.0	270.0
242	L16	2425.0	5000.0	-136.0	272	N15	2210.0	1050.0	330.0
243	L17	2425.0	4800.0	-136.0	273	N16	2410.0	1050.0	360.0
244	L18	2425.0	4600.0	-85.0	274	O01	2410.0	1400.0	375.0
245	L19	2425.0	4400.0	-14.0	275	O02	2425.0	1610.0	340.0
246	L20	2425.0	4200.0	66.0	276	O03	2435.0	1810.0	300.0
247	L21	2425.0	4000.0	157.0	277	O04	2435.0	2010.0	370.0
248	M01	1710.0	3610.0	-106.0	278	O05	2435.0	2200.0	260.0
249	M02	1610.0	3610.0	-148.0	279	O06	2450.0	2410.0	210.0
250	M03	1410.0	3610.0	-167.0	280	O07	2450.0	2600.0	220.0
251	M04	1225.0	3610.0	-207.0	281	O08	2485.0	2810.0	170.0
252	M05	1010.0	3625.0	-226.0	282	O09	2485.0	3000.0	170.0
253	M06	810.0	3635.0	-226.0	283	O10	2485.0	3210.0	120.0
254	M07	610.0	3650.0	-255.0	284	O11	2500.0	3400.0	250.0
255	M08	410.0	3650.0	-274.0	285	O12	2510.0	3600.0	120.0
256	M09	225.0	3675.0	-264.0	286	O13	2525.0	3800.0	90.0
257	M10	25.0	3710.0	-283.0	287	O14	2560.0	4000.0	-30.0
258	N01	0.0	1050.0	560.0	288	O15	2625.0	4200.0	-100.0
259	N02	210.0	1050.0	600.0	289	O16	2510.0	4200.0	0.0
260	N03	410.0	1050.0	520.0	290	P01	0.0	4800.0	-280.0
261	N04	610.0	1050.0	570.0	291	P02	0.0	5000.0	-280.0
262	N05	810.0	1050.0	490.0	292	P03	0.0	5200.0	-310.0
263	N06	1010.0	1050.0	530.0	293	P04	0.0	5410.0	-340.0
264	N07	1100.0	1050.0	470.0	294	P05	0.0	5600.0	-330.0
265	N08	1210.0	1050.0	350.0	295	P06	0.0	5800.0	-250.0
266	N09	1400.0	1050.0	200.0	296	P07	0.0	6010.0	-190.0
267	N10	1500.0	1050.0	190.0	297	P08	0.0	6200.0	-110.0
268	N11	1600.0	1050.0	230.0	298	P09	0.0	6410.0	-50.0
269	N12	1700.0	1050.0	270.0	299	P10	0.0	6600.0	-60.0
270	N13	1810.0	1050.0	200.0	300	P11	0.0	6800.0	-80.0

Corrected vertical magnetic intensity survey data.

#	LINE #	X	Y	Z	#	LINE #	X	Y	Z
301	P12	0.0	7000.0	-120.0	331	Q21	1225.0	3360.0	-160.0
302	P13	0.0	7210.0	130.0	332	Q22	1210.0	3185.0	-130.0
303	P14	0.0	7300.0	2575.0	333	Q23	1225.0	2950.0	-90.0
304	P15	0.0	7410.0	5200.0	334	Q24	1225.0	2760.0	-50.0
305	P16	225.0	7410.0	4700.0	335	Q25	1210.0	2560.0	-30.0
306	P17	425.0	7410.0	2425.0	336	Q26	1210.0	2360.0	-30.0
307	P18	625.0	7410.0	1125.0	337	R01	6000.0	4285.0	-157.0
308	P19	825.0	7410.0	820.0	338	R02	6000.0	4235.0	-137.0
309	P20	1025.0	7410.0	3200.0	339	R03	6000.0	4185.0	-215.0
310	P21	1225.0	7410.0	4000.0	340	R04	6000.0	4085.0	-235.0
311	Q01	1225.0	7300.0	1820.0	341	R05	6000.0	3985.0	-214.0
312	Q02	1225.0	7125.0	20.0	342	R06	6000.0	3900.0	-212.0
313	Q03	1225.0	6935.0	-80.0	343	R07	6000.0	3800.0	-212.0
314	Q04	1210.0	6750.0	-30.0	344	R08	6000.0	3585.0	-201.0
315	Q05	1210.0	6550.0	0.0	345	R09	6000.0	3400.0	-188.0
316	Q06	1210.0	6360.0	-30.0	346	R10	6000.0	3185.0	-157.0
317	Q07	1210.0	6160.0	-35.0	347	R11	5985.0	2985.0	-134.0
318	Q08	1210.0	5950.0	-100.0	348	R12	5985.0	2785.0	-132.0
319	Q09	1210.0	5750.0	-180.0	349	R13	5985.0	2585.0	-121.0
320	Q10	1225.0	5560.0	-230.0	350	R14	6000.0	2385.0	-19.0
321	Q11	1225.0	5350.0	-250.0	351	R15	6000.0	2200.0	65.0
322	Q12	1225.0	5150.0	-280.0	352	R16	6000.0	2000.0	76.0
323	Q13	1210.0	4960.0	-310.0	353	R17	6000.0	1800.0	198.0
324	014	1210.0	4750.0	-300.0	354	R18	6000.0	1600.0	296.0
325	Q15	1225.0	4550.0	-300.0	355	R19	6000.0	1385.0	471.0
326	Q16	1225.0	4360.0	-280.0	356	R20	6000.0	1185.0	713.0
327	Q17	1210.0	4150.0	-260.0	357	R21	6000.0	1000.0	905.0
328	Q18	1225.0	3950.0	-250.0	358	R22	6000.0	800.0	1181.0
329	Q19	1225.0	3760.0	-250.0	359	R23	6000.0	600.0	1657.0
330	Q20	1225.0	3560.0	-200.0	360	S01	4600.0	3585.0	-170.0

Corrected vertical magnetic intensity survey data.

#	LINE #	X	Y	Z	#	LINE #	X	Y	Z
361	S02	4400.0	3585.0	-150.0	391	T17	4800.0	200.0	3970.0
362	S03	4200.0	3585.0	-90.0	392	T18	4800.0	100.0	3920.0
363	S04	4000.0	3585.0	-40.0	393	U01	4200.0	3885.0	-167.0
364	S05	3800.0	3585.0	-40.0	394	U02	4200.0	3700.0	-185.0
365	S06	3600.0	3585.0	-24.0	395	U03	4200.0	3600.0	-90.0
366	S07	3400.0	3585.0	-30.0	396	U04	4200.0	3485.0	-93.0
367	S08	3200.0	3585.0	70.0	397	U05	4200.0	3285.0	-22.0
368	S09	3000.0	3585.0	220.0	398	U06	4200.0	3100.0	80.0
369	S10	2800.0	3585.0	40.0	399	U07	4200.0	2900.0	43.0
370	S11	2610.0	3585.0	120.0	400	U08	4200.0	2685.0	25.0
371	S12	2410.0	3585.0	-80.0	401	U09	4200.0	2500.0	229.0
372	S13	2210.0	3585.0	60.0	402	V01	8375.0	0.0	3489.0
373	S14	2010.0	3585.0	120.0	403	V02	8375.0	85.0	3389.0
374	S15	1825.0	3585.0	-60.0	404	V03	8375.0	185.0	3456.0
375	T01	4800.0	3400.0	-157.0	405	V04	8385.0	300.0	3386.0
376	T02	4800.0	3200.0	-164.0	406	V05	8385.0	385.0	3460.0
377	T03	4800.0	3000.0	-75.0	407	V06	8385.0	500.0	4035.0
378	T04	4800.0	2800.0	-18.0	408	V07	8385.0	575.0	4062.0
379	T05	4800.0	2600.0	23.0	409	V08	8400.0	685.0	4550.0
380	T06	4800.0	2385.0	21.0	410	V09	8425.0	785.0	4948.0
381	T07	4800.0	2200.0	70.0	411	V10	8435.0	885.0	4520.0
382	T08	4800.0	1985.0	205.0	412	V11	8450.0	985.0	4320.0
383	T09	4800.0	1800.0	322.0	413	V12	8475.0	1085.0	4320.0
384	T10	4800.0	1600.0	441.0	414	V13	8485.0	1185.0	4020.0
385	T11	4800.0	1400.0	808.0	415	V14	8510.0	1285.0	3870.0
386	T12	4800.0	1200.0	856.0	416	V15	8525.0	1400.0	3870.0
387	T13	4800.0	1000.0	1084.0	417	V16	8535.0	1485.0	2720.0
388	T14	4800.0	800.0	1774.0	418	V17	8560.0	1585.0	2195.0
389	T15	4800.0	600.0	3445.0	419	V18	8575.0	1685.0	1460.0
390	T16	4800.0	400.0	3496.0	420	V19	8585.0	1785.0	1095.0

Corrected vertical magnetic intensity survey data.

#	LINE #	X	Y	Z	#	LINE #	X	Y	Z
421	V20	8610.0	1885.0	1027.0	451	W17	5010.0	4185.0	-250.0
422	V21	8635.0	1985.0	770.0	452	W18	4810.0	4185.0	-356.0
423	V22	8650.0	2085.0	470.0	453	W19	4250.0	4185.0	-250.0
424	V23	8700.0	2185.0	345.0	454	W20	4000.0	4185.0	-210.0
425	V24	8710.0	2285.0	220.0	455	W21	3800.0	4185.0	-125.0
426	V25	8735.0	2385.0	195.0	456	W22	3410.0	4200.0	-50.0
427	V26	8775.0	2485.0	95.0	457	W23	3200.0	4200.0	-175.0
428	V27	8800.0	2585.0	20.0	458	W24	2800.0	4200.0	-75.0
429	V28	8825.0	2675.0	-30.0	459	X01	8285.0	3585.0	-80.0
430	V29	8825.0	2775.0	20.0	460	X02	8100.0	3585.0	-70.0
431	V30	8860.0	2885.0	-130.0	461	X03	7885.0	3585.0	-130.0
432	V31	8885.0	2985.0	-130.0	462	X04	7700.0	3585.0	-180.0
433	V32	8885.0	3075.0	-130.0	463	X05	7485.0	3585.0	-130.0
434	V33	8885.0	3185.0	-130.0	464	X06	7300.0	3585.0	-180.0
435	W01	8185.0	4185.0	80.0	465	X07	7085.0	3585.0	-130.0
436	W02	8000.0	4185.0	110.0	466	X08	6900.0	3585.0	-180.0
437	W03	7785.0	4185.0	-30.0	467	X09	6685.0	3585.0	-155.0
438	W04	7600.0	4185.0	-50.0	468	X10	6500.0	3585.0	-180.0
439	W05	7400.0	4185.0	-120.0	469	X11	6310.0	3585.0	-220.0
440	W06	7185.0	4200.0	-150.0	470	X12	6100.0	3585.0	-205.0
441	W07	7000.0	4185.0	-175.0	471	X13	5900.0	3585.0	-180.0
442	W08	6785.0	4185.0	-150.0	472	X14	5700.0	3585.0	-155.0
443	W09	6600.0	4185.0	-150.0	473	X15	5500.0	3585.0	-130.0
444	W10	6400.0	4185.0	-200.0	474	X16	5100.0	3585.0	-180.0
445	W11	6185.0	4185.0	-175.0	475	X17	4910.0	3585.0	-180.0
446	W12	6000.0	4185.0	-215.0	476	Y01	5975.0	4300.0	-172.0
447	W13	5800.0	4185.0	-175.0	477	Y02	5935.0	4300.0	-162.0
448	W14	5600.0	4185.0	-210.0	478	Y03	5875.0	4300.0	-202.0
449	W15	5400.0	4185.0	-230.0	479	Y04	5835.0	4300.0	-312.0
450	W16	5200.0	4185.0	-150.0	480	Y05	5775.0	4300.0	-182.0

Corrected vertical magnetic intensity survey data.

#	LINE#	X	Y	Z	#	LINE#	X	Y	Z
481	Y06	5735.0	4285.0	-212.0	511	Y36	4175.0	4285.0	-233.0
482	Y07	5675.0	4285.0	-202.0	512	Y37	4135.0	4285.0	-291.0
483	Y08	5635.0	4285.0	-203.0	513	Y38	4085.0	4285.0	-188.0
484	Y09	5575.0	4285.0	-163.0	514	Y39	4035.0	4285.0	-248.0
485	Y10	5525.0	4285.0	-253.0	515	Y40	3975.0	4285.0	-208.0
486	Y11	5485.0	4300.0	-164.0	516	Y41	3925.0	4285.0	-172.0
487	Y12	5425.0	4285.0	-154.0	517	Y42	3875.0	4285.0	-162.0
488	Y13	5375.0	4285.0	-234.0	518	Y43	3835.0	4285.0	-182.0
489	Y14	5325.0	4285.0	-224.0	519	Y44	3785.0	4285.0	-132.0
490	Y15	5285.0	4285.0	-224.0	520	Y45	3735.0	4285.0	-158.0
491	Y16	5235.0	4285.0	-154.0	521	Y46	3700.0	4285.0	-137.0
492	Y17	5175.0	4285.0	-165.0	522	Z01	4800.0	4500.0	-382.0
493	Y18	5135.0	4285.0	-225.0	523	Z02	4800.0	4450.0	-489.0
494	Y19	5085.0	4285.0	15.0	524	Z03	4800.0	4400.0	-668.0
495	Y20	5035.0	4285.0	-215.0	525	Z04	4800.0	4335.0	-1039.0
496	Y21	4985.0	4285.0	-245.0	526	Z05	4800.0	4285.0	-369.0
497	Y22	4925.0	4285.0	-255.0	527	Z06	4800.0	4235.0	-363.0
498	Y23	4875.0	4285.0	-279.0	528	Z07	4800.0	4185.0	-356.0
499	Y24	4825.0	4285.0	-369.0	529	Z08	4800.0	4085.0	-269.0
500	Y25	4775.0	4285.0	-371.0	530	Z09	4800.0	3985.0	-208.0
501	Y26	4725.0	4285.0	-290.0	531	Z10	4800.0	3885.0	-118.0
502	Y27	4675.0	4285.0	-290.0	532	Z11	4800.0	3785.0	-128.0
503	Y28	4625.0	4285.0	-440.0	533	Z12	4800.0	3635.0	-147.0
504	Y29	4585.0	4285.0	-290.0	534	VA1	8485.0	3260.0	-180.0
505	Y30	4525.0	4285.0	-290.0	535	VA2	8375.0	3375.0	-180.0
506	Y31	4475.0	4285.0	-280.0	536	VA3	8375.0	3475.0	-180.0
507	Y32	4425.0	4285.0	-270.0	537	VA4	8375.0	3585.0	-180.0
508	Y33	4335.0	4285.0	-249.0	538	VA5	8375.0	3675.0	-105.0
509	Y34	4285.0	4285.0	-289.0	539	VA6	8375.0	3785.0	-90.0
510	Y35	4235.0	4285.0	-179.0	540	VA7	8375.0	3875.0	-30.0

Corrected vertical magnetic intensity survey data.

#	LINE#	X	Y	Z	#	LINE	X	Y	Z
541	VB1	7785.0	1085.0	4500.0	558	01B	4610.0	4550.0	-131.0
542	01A	4400.0	4750.0	-155.0	559	02B	4610.0	4450.0	-393.0
543	02A	4400.0	4685.0	-155.0	560	03B	4600.0	4400.0	-323.0
544	03A	4400.0	4650.0	-165.0	561	04B	4600.0	4335.0	-263.0
545	04A	4400.0	4585.0	-285.0	562	05B	4600.0	4285.0	-263.0
546	05A	4400.0	4550.0	-225.0	563	06B	4600.0	4235.0	-222.0
547	06A	4400.0	4500.0	-265.0	564	07B	4600.0	4185.0	-313.0
548	07A	4400.0	4450.0	-265.0	565	08B	4600.0	4135.0	-193.0
549	08A	4400.0	4285.0	-244.0	566	09B	4600.0	4100.0	-203.0
550	09A	4400.0	4235.0	-234.0	567	10B	4600.0	4035.0	-223.0
551	10A	4400.0	4185.0	-256.0	568	11B	4600.0	3985.0	-163.0
552	11A	4400.0	4135.0	-216.0	569	12B	4600.0	3935.0	-184.0
553	12A	4400.0	4085.0	-216.0	570	13B	4600.0	3835.0	-204.0
554	13A	4400.0	4035.0	-236.0	571	01C	8375.0	2985.0	-163.0
555	14A	4400.0	3985.0	-226.0	572	02C	8175.0	2985.0	-104.0
556	15A	4400.0	3935.0	-196.0	573	03C	7985.0	2985.0	-145.0
557	16A	4400.0	3835.0	-166.0					

APPENDIX C

The Remanent Magnetization Orientation and Intensity for Each Sample: NRM, Thermally Cleaned, and A.C. Cleaned.

Sample Site A

	(NRM)			(Thermally Cleaned)			(A.C. Cleaned)		
Sample	Dec.	Inc.	Intensity X 10^{-3} emu/cm^3	Dec.	Inc.	Intensity X 10^{-3} emu/cm^3	Dec.	Inc.	Intensity X 10^{-3} emu/cm^3
A(1)	126.8	-28.7	1.56	---	---	---	144.1	-22.0	10.70
A(2)	135.1	-27.7	1.80	---	---	---	156.7	-26.0	12.35
A(3)	137.1	-27.6	.65	156.6	-20.1	6.49	---	---	---
A(4)	129.6	-61.2	.74	133.8	-7.3	3.80	---	---	---
A(5)	138.4	-27.3	.54	166.8	66.9	4.97	---	---	---
A(6)	144.2	-14.5	---	157.2	-13.2	---	---	---	---
Average	135.8	-31.0	1.06	151.1	-26.6		117.0	-30.3	

Average Cleaned Intensity = .76 X 10^{-3} emu/cm^3

Sample Site B

	(NRM)			(Thermally Cleaned)			(A.C. Cleaned)		
Sample	Dec.	Inc.	Intensity X 10^{-3} emu/cm^3	Dec.	Inc.	Intensity X 10^{-3} emu/cm^3	Dec.	Inc.	Intensity X 10^{-3} emu/cm^3
B(1)	70.6	-42.5	84.0	---	---	---	102.7	-42.0	31.4
B(2)	69.9	-40.7	59.5	81.8	-24.0	59.4	---	---	---
B(3)	73.6	-39.9	55.9	73.0	-42.2	49.2	---	---	---
B(4)	65.8	-28.7	60.9	74.5	-42.3	60.5	---	---	---
B(5)	124.4	-40.5	47.5	94.9	-44.7	41.2	---	---	---
B(6)	85.0	-42.8	49.7	82.2	-44.1	42.0	---	---	---
Average	80.5	-40.0	59.5	81.2	-39.7		102.7	-42.0	

Average Cleaned Intensity 47.3 x 10^{-3} emu/cm^3

Sample Site C

	(NRM)			(Thermally Cleaned)			(A.C. Cleaned)		
Sample	Dec.	Inc.	Intensity X 10^{-3} emu/cm^3	Dec.	Inc.	Intensity X 10^{-3} emu/cm^3	Dec.	Inc.	Intensity X 10^{-3} emu/cm^3
C(1)	68.9	-46.5	2.84	---	---	---	66.9	-42.0	1.62
C(2)	67.6	-38.3	3.92	69.3	-26.1	3.92	---	---	---
C(3)	62.6	-33.0	21.26	64.2	-34.1	20.84	---	---	---
C(4)	67.8	-47.1	4.06	65.4	-39.1	3.95	---	---	---
C(5)	62.1	-52.5	3.66	57.1	-43.2	3.36	---	---	---
C(6)	55.8	-43.1	4.70	54.7	-44.6	4.57	---	---	---
Average	64.1	-43.0	6.74	62.6	-37.5		66.9	-42.0	

Average Cleaned Intensity = 6.52 x 10^{-3} emu/cm^3

Sample Site D

	(NRM)			(Thermally Cleaned)			(A.C. Cleaned)		
Sample	Dec.	Inc.	Intensity X 10^{-5} emu/cm^3	Dec.	Inc.	Intensity X 10^{-5} emu/cm^3	Dec.	Inc.	Intensity X 10^{-5} emu/cm^3
D(1)	58.8	-46.9	11.23	61.2	-59.2	11.91	---	---	---
D(2)	53.6	-47.8	10.38	87.2	-65.4	14.71	---	---	---
Average	56.1	-52.4	10.81	72.8	-62.9	13.34			

Sample Site E

	(NRM)			(Thermally Cleaned)			(A.C. Cleaned)		
Sample	Dec.	Inc.	Intensity X 10^{-5} emu/cm^3	Dec.	Inc.	Intensity X 10^{-5} emu/cm^3	Dec.	Inc.	Intensity X 10^{-5} emu/cm^3
E(1)	1.1	-28.7	11.98	---	---	14.3	---	---	---
E(2)	17.3	-57.2	12.73	67.9	-58.8	19.2	---	---	---
E(3)	86.6	-43.2	34.22	98.5	-33.5	37.57	---	---	---
E(4)	12.7	-60.8	19.28	27.9	-68.9	24.20	---	---	---
E(5)	20.2	-49.6	12.10	72.3	-57.1	20.51	---	---	---
E(6)	69.5	-71.6	---	---	---	---	---	---	---
Average	32.0	-57.0	81.10	74.4	-56.9	23.2			

Sample Site F

	(NRM)			(Thermally Cleaned)			(A.C. Cleaned)		
Sample	Dec.	Inc.	Intensity X 10^{-3} emu/cm^3	Dec.	Inc.	Intensity X 10^{-3} emu/cm^3	Dec.	Inc.	Intensity X 10^{-3} emu/cm^3
F(1)	176.8	-24.0	88.3	---	---	---	178.8	-23.1	88.3
F(2)	139.2	-16.7	122.3	152.4	-10.3	146.5	---	---	---
F(3)	141.4	-14.7	115.7	142.4	-14.7	97.5	---	---	---
F(4)	138.0	-47.5	84.4	134.2	-48.3	80.0	---	---	---
F(5)	148.0	-46.4	1.8	160.8	-22.4	2.3	---	---	---
Average	149.0	-28.0	82.5	148.8	-24.0		178.8	-23.1	

Average Cleaned Intensity = 82.9 x 10^{-3} emu/cm^3

Sample Site G

	(NRM)			(Thermally Cleaned)			(A.C. Cleaned)		
Sample	Dec.	Inc.	Intensity X 10^{-3} emu/cm^3	Dec.	Inc.	Intensity X 10^{-3} emu/cm^3	Dec.	Inc.	Intensity X 10^{-3} emu/cm^3
G(1)	187.9	-81.9	2.31	Random	Random		Random	Random	
G(2)	78.8	-6.2	.74						
G(3)	57.0	-5.4	3.27						
G(4)	233.6	-33.8	.68						
G(5)	79.5	-5.9	1.31						
G(6)	325.5	-68.2	3.39						
Average	72.6	-54.5	1.95						

Sample Site 1A

	(NRM)			(Thermally Cleaned)			(A.C. Cleaned)		
Sample	Dec.	Inc.	Intensity X 10^{-3} emu/cm^3	Dec.	Inc.	Intensity X 10^{-3} emu/cm^3	Dec.	Inc.	Intensity X 10^{-3} emu/cm^3
1A(1)	59.1	-50.2	3.25	---	---	---	58.2	-47.6	3.31
1A(2)	55.8	-37.5	3.38	52.5	-33.9	3.80	---	---	---
1A(3)	49.7	-55.4	2.90	45.0	-54.2	3.06	---	---	---
1A(4)	56.4	-30.0	4.35	56.8	-28.7	4.58	---	---	---
Average	54.9	-42.0		52.2	-38.9		58.2	-47.6	

Average Cleaned Intensity = 3.68 x 10^{-3} emu/cm^3

Sample Site 2A

	(NRM)			(Thermally Cleaned)			(A.C. Cleaned)		
Sample	Dec.	Inc.	Intensity X 10^{-3} emu/cm^3	Dec.	Inc.	Intensity X 10^{-3} emu/cm^3	Dec.	Inc.	Intensity X 10^{-3} eum/cm^3
2A(1)	157.1	-65.9	3.13	---	---	---	149.9	-66.9	3.17
2A(2)	154.0	-70.9	4.16	151.3	-72.1	4.26	---	---	---
2A(3)	183.2	-73.4	3.41	165.9	-78.8	3.42	---	---	---
2A(4)	133.0	-38.6	2.02	132.6	-41.1	1.94	---	---	---
2A(5)	93.5	-69.2	4.28	88.7	-68.8	4.42	---	---	---
2A(6)	100.3	-84.6	4.16	---	---	---	---	---	---
Average	138.0	-69.0		130.8	-67.4		149.9	-66.9	

Average Cleaned Intensity =3.45 x 10^{-3} emu/cm^3

Sample Site 3A

	(NRM)			(Thermally Cleaned)			(A.C. Cleaned)		
Sample	Dec.	Inc.	Intensity X 10^{-5} emu/cm^3	Dec.	Inc.	Intensity X 10^{-5} emu/cm^3	Dec.	Inc.	Intensity X 10^{-5} emu/cm^3
3A(1)	114.7	-67.3	85.0	123.1	-64.9	77.0	---	---	---
3A(2)	70.9	-56.7	42.8	71.6	-87.3	47.7	---	---	---
3A(3)	---	---	44.8	---	---	19.6	---	---	---
3A(4)	86.7	-56.1	52.9	89.6	-61.0	62.4	---	---	---
3A(5)	86.6	-60.8	56.1	90.6	-58.3	62.4	---	---	---
Average	82.7	-62.5		98.9	-68.5	53.9			

APPENDIX D

Computer Model Listing

SCOOPFMT

```
100=PHILLIPS,PN606213 ,RG1,CM120000,JC1500.
110=ATTACH,TAPE88,LEVELONE,PW=MAG.
120=ATTACH,PREFIX,BINPREFIX,PW=MAG
130=ATTACH,ONE,SHALOCI,PW-MAG.
140=PREFIX.
150=REWIND,TAPE99.
160=ONE,TAPE99.
170=CATALOG,TAPE7,WES10,PW=MAG,ID=WES,RP=30.
180=REWIND,TAPE7.
190=COPY,TAPE7,OUT.
200=DISPOSE,OUT,PR.
200,000001=*EOROO
220=00. 70.
230=*EOR.
```

PREFIX

```
100=        PROGRAM PREFIX (INPUT,TAPE77=INPUT,TAPE88,TAPE99,OUTPUT=TAPE99)
110=        DIMENSION X(2,45),Y(2,45),Z(2,45),EXTRA(13),OPTIONS(5),PROP(4,46)
120=        DATA RADCONV/57.2957995/
130=        READ(77,1) AZIMUTH,DIP
140=        READ(88,2) (EXTRA(I),I=1,3)
150=        READ(88,3) IROW,ICOL,EXTRA(4)
160=        N=1
170=30      CONTINUE
180=        READ(88,15) FLAG,(PROP(I,N),I=1,4)
190=        IF(FLAG,EQ.8HEND DATA)GO TO 20
200=        READ(88,5) (X(I,N),Y(I,N),Z(I,N),I=1,2)
210=        N=N+1
220=        GO TO 30
230=20      CONTINUE
240=        READ(88,6) (OPTIONS(I),I=1,5)
260=        DIP=DIP/RADCONV
270=        AZIMUTH=AZIMUTH/RADCONV
275=        N=N-1
280=        DO 100 I=1,N
300=        RHO=Z(1,I)/TAN(DIP)
310=        X(1,I)=COS(AZIMUTH)*RHO+X(1,I)
315=        X(2,I)=COS(AZIMUTH)*RHO+X(2,I)
320=        Y(1,I)=SIN(AZIMUTH)*RHO+Y(1,I)
325=        Y(2,I)=SIN(AZIMUTH)*RHO+Y(2,I)
330=100     CONTINUE
340=        WRITE(99,2) (EXTRA(I),I=1,3)
350=        WRITE(99,3) IROW,ICOL,EXTRA(4)
360=        DO 200 J=1,N
370=        WRITE(99,4) (PROP(I,J),I=1,4)
```

```
380=200     WRITE(99,5) (X(I,J),Y(I,J),Z(I,J),I=1,2)
390=        WRITE(99,10)
400=        WRITE(99,6) (OPTIONS(I),I=1,5)
410=        WRITE(99.7) TITLE
420=1       FORMAT(F4.0,F3.0)
430=2       FORMAT(3F5.1)
440=3       FORMAT(2I2,F5.3)
450=4       FORMAT(10X,4F13.1)
460=5       FORMAT(6F5.2)
470=6       FORMAT(5I1)
480=7       FORMAT(8A10)
490=15      FORMAT(A10,4F13.1)
500=10      FORMAT(8HEND DATA)
510=        STOP
520=        END
```

LEVELONE

```
10=  1.0 84.00 46.5
20=20201.0
1000=            100.0        296.0        322.8        8.4
1100=8.7508.750.050012.2512.25.5000
1110=            100.0        296.0        322.8        8.4
1200=9.2508.325.050011.758.750.5000
1210=            100.0        296.0        322.8        8.4
1300=12.259.250.050012.6211.75.5000
1310=            100.0        296.0        322.8        8.4
1400=9.25012.25.050011.7512.62.5000
1410=            100.0        296.0        322.8        8.4
1500=8.3259.250.05008.75011.75.5000
1510=            100.0        296.0        322.8        8.4
1600=10.008.000.050011.008.325.5000
1610=            100.0        296.0        322.8        8.4
1700=12.6310.00.050013.0011.00.5000
1710=            100.0        296.0        322.8        8.4
1800=10.0012.63.050011.0013.00.5000
1810=            100.0        296.0        322.8        8.4
1900=8.00010.00.05008.32511.00.5000
2000=            100.0        296.0        322.8        8.4
2010=8.7508.750.500012.2512.251.000
2020=            100.0        296.0        322.8        8.4
2030=9.2508.325.500011.758.7501.000
2040=            100.0        296.0        322.8        8.4
2050=12.259.250.500012.6211.751.000
2060=            100.0        296.0        322.8        8.4
2070=9.25012.25.500011.7512.621.000
2080=            100.0        296.0        322.8        8.4
2090=8.3259.250.50008.75011.751.000
2100=            100.0        296.0        322.8        8.4
```

```
2110=10.008.000.500011.008.3251.000
2120=           100.0        296.0        322.8        8.4
2130=12.6310.00.500013.0011.001.000
2140=           100.0        296.0        322.8        8.4
2150=10.0012.63.500011.0013.001.000
2160=           100.0        296.0        322.8        8.4
2170=8.00010.00.50008.32511.001.000
3000=           100.0        296.0        322.8        8.4
3010=8.7508.7501.00012.2512.251.500
3020=           100.0        296.0        322.8        8.4
3030=9.2508.3251.00011.758.7501.500
3040=           100.0        296.0        322.8        8.4
3050=12.259.2501.00012.6211.751.500
3060=           100.0        296.0        322.8        8.4
3070=9.25012.251.00011.7512.621.500
3080=           100.0        296.0        322.8        8.4
3090=8.3259.2501.0008.75011.751.500
3100=           100.0        296.0        322.8        8.4
3110=10.008.0001.00011.008.3251.500
3120=           100.0        296.0        322.8        8.4
3130=12.6310.001.00013.0011.001.500
3140=           100.0        296.0        322.8        8.4
3150=10.0012.631.00011.0013.001.500
3160=           100.0        296.0        322.8        8.4
3170=8.00010.001.0008.32511.001.500
4000=           100.0        296.0        322.8        8.4
4010=8.7508.7501.50012.2512.252.000
4020=           100.0        296.0        322.8        8.4
4030=9.2508.3251.50011.758.7502.000
4040=           100.0        296.0        322.8        8.4
4050=12.259.2501.50012.6211.752.000
4060=           100.0        296.0        322.8        8.4
4070=9.25012.251.50011.7512.622.000
4080=           100.0        296.0        322.8        8.4
4090=8.3259.2501.5008.75011.752.000
4100=           100.0        296.0        322.8        8.4
4110=10.008.0001.50011.008.3252.000
4120=           100.0        296.0        322.8        8.4
4130=12.6310.001.50013.0011.002.000
4140=           100.0        296.0        322.8        8.4
4150=10.0012.631.50011.0013.002.000
4160=           100.0        296.0        322.8        8.4
4170=8.00010.001.5008.32511.002.000
5000=           100.0        296.0        322.8        8.4
5010=8.7508.7502.00012.2512.252.500
5020=           100.0        296.0        322.8        8.4
5030=9.2508.3252.00011.758.7502.500
5040=           100.0        296.0        322.8        8.4
5050=12.259.2502.00012.6211.752.500
5060=           100.0        296.0        322.8        8.4
5070=9.25012.252.00011.7512.622.500
5080=           100.0        296.0        322.8        8.4
5090=8.3259.2502.0008.75011.752.500
```

```
5100=              100.0          296.0          322.8          8.4
5110=10.008.0002.00011.008.3252.500
5120=              100.0          296.0          322.8          8.4
5130=12.6310.002.00013.0011.002.500
5140=              100.0          296.0          322.8          8.4
5150=10.0012.632.00011.0013.002.500
5160=              100.0          296.0          322.8          8.4
5170=8.00010.002.0008.32511.002.500
5200=END DATA
5210=    2
5220=SCOOPS MODEL.
```

APPENDIX E

Surface II Commands

Computer Model Contour Maps, Figures 14-17.

```
100=*JOBCARD*, CM100000, T500,RG2,JC1500.
110=ATTACH,TAPE 10,WES50,PW=MAG.
115=ATTACH,TAPE 11,LEVEL1,PW=MAG.
117=REWIND,TAPE 11.
120=REWIND TAPE 10.
130=ATTACH,SURFACE,BNOVSURF.
140=SURFACE.
140,000001=*EOR00
160=IDXY  400,10,3,2,3,1,,,,,"(2X,F10,2,2X,F10.2,2X,F10.2)"
170=GRID  0,39,39,2,4,1,0
180=OCTANT  1,1,1.4,1.8,4,11.25
190=CONT
195=LEVE  11,31,"(F7.1,1X,I1)"
200=CINT  2,,,,,.20,0,6,,
210=SIZC  1,11,11
220=BOX  1,0,1,0,1,0,0,1,0.20
230=DEVICE 4, "PHILLIPS"
240=PERFORM
250=STOP
```

Vertical Magnetic Intensity Contour Map (General Study Area), Figure 4

```
100=*JOBCARD*,CM100000,T500,RG1,JC3000.
110=ATTACH,TAPE 10,WESDATA3.
120=ATTACH,TAPE 11,WESDATA8.
130=REWIND TAPE 10,TAPE 11.
140=ATTACH,SURFACE,BNOVSURF.
150=SURFACE
160=*EOR
170=IDXY  573,10,4,2,3,4,,,,,'(A3,1X,F6.1,1X,F6.1,1X,F8.1)'
180=GRID  1,200,200,1,2,1,0
190=OCTANT  1,1,837,1800,4,11.25
200=CONT
210=LEVE  11,20,'(F7.1,1X,I1)'
220=CINT  2,,,,,0.075,0,4
230=SIZC  0,500,500
240=BOX  600,2,600,2,0,0,0,2,0.1
250=BXEX
260=DEVICE  5,'PHILLIPS'
270=PERFORM
280=STOP
```

Vertical Magnetic Intensity Contour Map (Detailed Map), Figure 5.

```
100=*JOBCARD*,CM100000,T500,RG1,JC3000.
110=ATTACH,TAPE 10,WESDATA5.
120=REWIND TAPE 10.
130=ATTACH,SURFACE,BNOVSURF.
140=SURFACE.
150=*EOR
160=IDXY  288,10,4,2,3,4,,,,,'(A3,1X,F6.1,1X,F6.1,1X,F8.1)'
170=GRID  1,25,25,1,2,1,0
180=OCTANT  1,1,700,1500,4,11.25
190=MLEVEL
200=CONT
210=CINT  0,0,100,0.1,0.05,0,4,5
220=SISC  0,500,500
230=BOX  600,2,500,2,0,2400,2400,2,0.1
240=BXEX
250=DEVICE  4,'PHILLIPS'
260=PERFORM
270=STOP
```

BIBLIOGRAPHY

BIBLIOGRAPHY

Beck, M. E., Jr., 1970. Paleomagnetism of Keweenawan Intrusive Rocks, Minnesota: Journal of Geophysical Research: vol 75, pp. 4985-4996.

Bhattacharyya, B. K., 1964. Magnetic Anomalies due to Prism-Shaped Bodies with Arbitrary Polarization: Geophysics, vol 29, pp. 517-531.

Blackett, P. M. S., 1956. Lectures on Rock Magnetism: Israel: Weiman Science Press.

Books, K. G., 1968. Remanent Magnetism as a Contributor to some Aeromagnetic Anomalies: Geophysics, vol 27, pp. 359-375.

Books, K. G., 1968. Magnetism of the Lowermost Keweenawan Lava Flows in the Lake Superior Area: U.S. Geological Survey professional Paper, 600-D, pp. D248-D254.

Cannon, W. F., and Gair, J. E., 1970. A Revision of Stratigraphic Nomenclatures for Middle Precambrian Rocks in Northern Michigan: Geol. Soc. Bull., vol 81, pp. 2843-2846.

Case, J. E. and Gair, J.E., 1965. Aeromagnetic Map of Parts of Marquette, Dickinson, Baraga, Alger, and Schoolcraft Counties, Michigan and its Geologic Interpretation: U.S. Geological Survey Geophysical Investigations Map GP 467.

Charles, E. J., 1965. Magnetism of Keweenawan Rocks Near Duluth, Minnesota: Geophysics, vol 30, pp. 858-874.

Chase, C. G. and Gilmer, T.H., 1973. Precambrian Plate Tectonics: The Mid- Continent Gravity High: Earth and Planetary Science Letters, vol 21, pp. 70-78.

Dubois, P. M., 1961. Paleomagnetism and Correlation of Keweenawan Rocks: Can. Geol. Surv., Bul. vol 71, p. 75.

Dubois, R.L. and Carey, W.W., 1964. Magnetic Investigations of a Ring Dike, Buell Park, Arizona: Geophysics, vol 29, pp. 553-564.

Girdler, R. W. and Peter, G., 1960. An Example of the Importance of Natural Remanent Magnetization in the Interpretation of Magnetic Anomalies: Geophysical Prospecting, vol 8, pp. 474-475.

Graham, J. W., 1953. Changes of Ferromagnetic Minerals and Their Bearing on Magnetic Properties of Rocks: Jour. Geophys. Research, vol 58, pp. 243-260.

Green, R., 1960. Remanent Magnetization and the Interpretation of Magnetic Anomalies: Geophysical Prospecting, vol 8, pp. 98-110.

Hayes, H. W. and Scharon, L., 1963. An Example of the Influence of Remanent Magnetization of Magnetic Intensity Measurements: Geophysics, vol 28, pp. 1037-1048.

Henderson, R. G., 1960. A Comprehensive System of Automatic Computation in Magnetic and Gravity Interpretation: Geophysics, vol 25, pp. 569-585.

Hinze, O'Hara, Secor, and Trow., 1966. Magnetic Properties;

Report of Investigation No. 12, Michigan Geologic Survey.

Irving, E. and McGlynn, J. C., 1976. Proterozoic Magnetostratigraphy and the tectonic evolution of Laurentia: Phil. Trans. R. Soc. London, vol A280, pp. 433-468.

Hood, P., 1963. Remanent Magnetism - A Neglected Factor in Aeromagnetic Interpretation: Canadian Mining Journal, vol 84(4), pp. 76-79.

Klasner, J. S., 1972. Style and Sequence of Deformation and Associated Metamorphism Due to the Penokian Orogeny in the Western Marquette Range, Northern Michigan: Doctor of Philosophy, Michigan Technological University.

Klasner, J. S. and Cannon, W. F., 1974. Geologic Interpretation of Gravity Profiles in the Western Marquette District, Northern Michigan: Geol. Soc. Bull.., vol 85, pp. 213-218.

Klasner, J. S., 1978. Penokean Deformation and Associated Metamorphism in the Western Marquette Range, Northern Michigan: Geol. Soc. Bull., vol 89, pp. 711-722.

McElhinny, M. W., 1973. Paleomagnetism and Plate Tectonics: Cambridge University Press, Cambridge.

Morris, W. J., 1978. Geochemistry and Origin of the Yellow Dog Plains Peridotite, Marquette County, Northern Michigan: M.S. Thesis, Michigan State University.

Nagata, T., 1953. Rock Magnetism: Tokyo: Maruzen Co. Ltd., 225 p.

Neel, L., 1955. Some Theoretical Aspects of Rock Magnetism: Advances in Physics, vol 4, pp. 191-243.

Palmer, H. C., 1970. Paleomagnetism and Correlation of some Middle Keweenawan Rocks, Lake Superior: Canadian J. of Earth Sciences, vol 7, pp. 1410-1436.

Park, F. B., 1968. Remanent Magnetism and the Anomaly at Cottoner Mountain, Madison County, Missouri: Geophysics, vol 33, pp. 613-620.

Sampson, R. J., 1978. SURFACE II Graphics System, Publication number one, Kansas Geologic Survey.

Shanabrook, D. C., 1978. A Geophysical and Geological Study of the Basement Complex Along the Peshekee River, Marquette County, Northern Michigan: M.S. Thesis, Michigan State University.

Strangeway, D. W., 1965. Interpretation of the Magnetic Anomalies over some Precambrain Dikes. Geophysics, vol 30, pp. 783-796.

Sutton, D. J. and Mumme, W. G., 1957. The Effect of Remanent Magnetization on Aeromagnetic Interpretation: Austrailian J. Physics, vol 10, pp. 547-557.

Torres, P. L., 1976. Gravity and Magnetic Study of Normally and Reversely Polarized Intrusions, Menominee County, Michigan: M.S. Thesis, Michigan State University.

Vacquier, V. A Machine Method for Computing the Magnitide and Direction of a Uniformly Magnetized Body from its Shape and Magnetic Survey: Proceeding of the Benedium Earth Magnetism Symposium, University of Pittsburgh Press.

Vincenz, S. A., 1968. Phenomenon of Partial Self-Reversal in Keweenawan Rocks, 1, Magnetization of Portage Lake Lavas: J. Geophysics. Res., vol 73, pp. 2729-2752.

Vincenz, S. A., and Yaskawa, K., 1968. Phenomenon of partial self-reversal in Keweenawan Rocks, 2, Magnetization of upper Keweenawan Lavas and Sediments and of Lower Keweenawan Dikes: J. Geophysics Res., vol 73, pp. 2729-1752.

Watkins, N. D., 1961. The Relative Contributions of Remanent and Induced Magnetism to the Observed Magnetic Field in Northeastern Alberta: Geophysical Prospecting, vol 9, pp. 423-426.

Whitehill, D. E., 1973. Automated Interpretation of Magnetic Anomalies using the Vertical Prism Model: Geophysics, vol 38, pp. 1070-1087.

Zietz, I. and Brooks, K. G., 1951. Aeromagnetic Interpretation and Remanent Magnetization: Journal of Geophysical Research, vol , p. 2572.

Zietz, I. and Andreasen G. E., 1967. Remanent Magnetization and Aeromagnetic Interpretation: Mining Geophysics, vol : SEG, Tulsa, pp. 569-590.

Zijderveld, J. D. A., 1967. A.C. Demagnetization of Rocks: Analysis of Results;